CHAPTER TWO

Magnetic Properties of Quasicrystals and Their Approximants

Zbigniew M. Stadnik*

Contents

1. Introduction

Solids are traditionally divided into two groups: crystalline and amorphous. The dramatic discovery of an icosahedral (*i*) Al–Mn alloy by Shechtman et al. (1984) extended this dichotomous division by introducing the notion of quasicrystals (QCs). These are compounds that possess a new

*Corresponding author. Tel.: +1-613-5625800
E-mail address: stadnik@uottawa.ca
Department of Physics, University of Ottawa, Ottawa, Ontario, Canada

Handbook of Magnetic Materials, Volume 21
ISSN 1567-2719, http://dx.doi.org/10.1016/B978-0-444-59593-5.00002-7

type of long-range translational order, quasiperiodicity, and a noncrystallographic orientational order associated with the crystallographically forbidden 5-fold, 8-fold, 10-fold, and 12-fold symmetry axes (Janot, 1994; Stadnik, 1999; Steurer and Deloudi, 2009).

To date, QCs have been discovered in more than a 100 ternary and binary intermetallic alloys (Steurer, 2004; Steurer and Deloudi, 2008). More than half of them are metastable, that is, they can only be obtained by rapid solidification. All known QCs are divided, according to their diffraction symmetry, into two classes (Steurer and Deloudi, 2008). The first class consists of polygonal (octagonal, decagonal (*d*), dodecagonal) QCs that are periodic along one direction. The other class consists of the most prevalent *i* QCs that have no periodicity along any direction. Only a few octagonal and dodecagonal QCs are known, and they are all metastable (Steurer, 2004).

Unlike crystalline compounds that are packed with identical unit cells in 3D space, QCs lack such units. Their structure must therefore be described using higher dimensional crystallography (Steurer and Deloudi, 2009). This involves describing QCs as periodic structures in 5D space (for polygonal QCs) or in 6D space (for *i* QCs). The 3D structure of a QC is then obtained as an irrational cut of the *n*D hypercrystal (Steurer and Deloudi, 2009; Yamamoto and Takakura, 2008).

Approximants (APs) are crystalline alloys in which the arrangements of atoms within their unit cells closely approximate the local atomic structures in QCs (Goldman and Kelton, 1993). In the higher dimensional description, they result from rational cuts of the *n*D hypercrystals. In analogy to the fact that the golden mean $\tau = \left(1+\sqrt{5}\right)/2$ can be approximated by its successive APs 1/1, 2/1, 3/2, 5/3, …, one can have 1/1, 2/1, 3/2, 5/3, … APs (Goldman and Kelton, 1993). Studies of the structure and physical properties of APs are important in efforts to elucidate the local atomic structure of QCs and their corresponding physical properties.

An extensive review of the magnetic properties of QCs by O'Handley et al. (1991) covered the literature up to 1989. Here, the literature from 1990 to 2011 is reviewed.

2. Magnetism in QCs

The possibility of the existence of long-range magnetic order in QCs is one of the main questions in the physics of these alloys. Initial intuition suggests that quasiperiodicity necessarily leads to geometrical frustration and is therefore incompatible with long-range magnetic order. However, there are numerous theoretical studies that suggest that long-range magnetic order in QCs should be possible. Although a magnetic-group analysis indicates that ferromagnetism is incompatible with the *i* symmetry

(Velikov et al., 2005a), symmetry-based arguments clearly show (Lifshitz, 1998, 2000; Lifshitz and Mandel, 2004; Mandel and Lifshitz, 2004) that quasiperiodicity does not disallow long-range antiferromagnetic order in QCs.

Using the Ising model on various quasiperiodic lattices, a rich family of different types of quasiperiodic magnetic order (ferromagnetic, antiferromagnetic, and ferrimagnetic) was predicted (Bhattacharjee et al., 1987; Duneau et al., 1991; Godrèche et al., 1986; Matsuo et al., 2000, 2002, 2005, 2007; Okabe and Niizeki, 1988a,b; Wen et al., 2008). Also, theoretical calculations based on the XY model indicate the possibility of the existence of long-range quasiperiodic magnetic order (Hermisson, 2000; Ledue et al., 1993; Reid et al., 1998). A complicated long-range quasiperiodic magnetic order is predicted by calculations based on the Heisenberg model (Jagannathan, 2004, 2005; Jagannathan and Szallas, 2009; Jagannathan et al., 2007; Szallas and Jagannathan, 2008; Szallas et al., 2009; Vedmedenko, 2004, 2005; Vedmedenko et al., 2003, 2004, 2006; Wessel and Milat, 2005; Wessel et al., 2003). Calculations based on the Hubbard model also predict the antiferromagnetic quasiperiodic magnetic order (Hida, 2001; Jagannathan and Schulz, 1997).

The theoretical arguments for the existence of a long-range quasiperiodic magnetic order are thus overwhelming. And as will be shown later, such a long-range quasiperiodic magnetic order has yet to be found in real QCs.

3. Al-Based QCs and APs

3.1. Al–TM (transition metal)–Fe system

Discovered in 1987 (Tsai et al., 1987), the *i* $Al_{65}Cu_{20}Fe_{15}$ QC was one of the first thermodynamically stable QCs possessing a high degree of structural perfection comparable to that found in the best periodic alloys. The early magnetic measurements of this QC (Matsuo et al., 1988; Stadnik et al., 1989) indicated, surprisingly, that it is diamagnetic at low temperatures. This was later confirmed in many subsequent studies on high-quality polygrain and single-grain samples. Figures 2.1 and 2.2 illustrate the temperature dependence of the magnetic susceptibility χ of the polygrain and single-grain *i* Al–Cu–Fe QCs, respectively. A diamagnetic behavior is evident in the temperature range 2–300 K, although a slight upturn of χ below 38 K for the polygrain sample is indicative of a paramagnetic contribution due to a parasitic crystalline impurity or to structural defects (Klein et al., 1991). A linear dependence of χ with $\sqrt{T}$ observed for the polygrain sample below 40 K (Fig. 2.1), which was taken as evidence for enhanced electron–electron interaction effects (Klein et al., 1990, 1991), is clearly not present for the single-grain sample (Fig. 2.2).

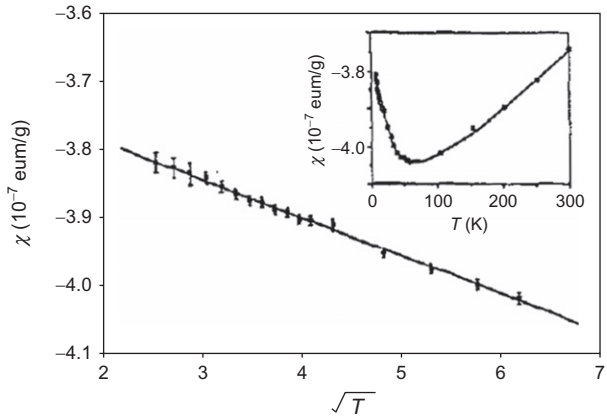

Figure 2.1 The temperature dependence of the magnetic susceptibility of the polygrain *i* $Al_{63}Cu_{25}Fe_{12}$ QC (Klein et al., 1990).

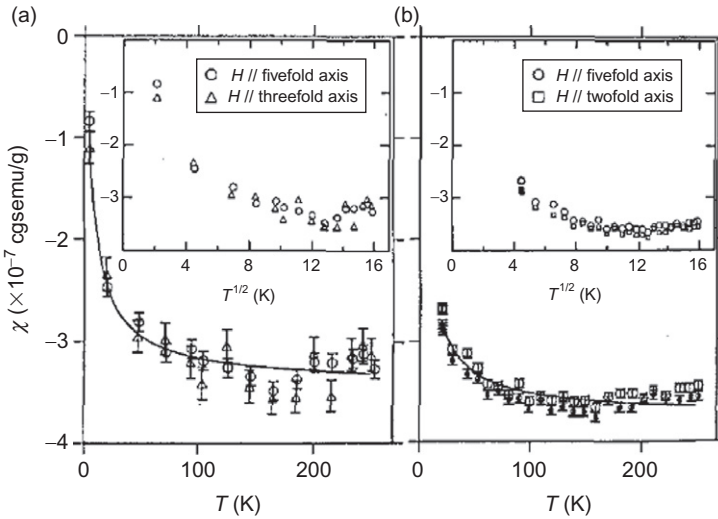

Figure 2.2 The temperature dependence of the magnetic susceptibility of the single-grain *i* $Al_{66.3}Cu_{20.4}Fe_{13.3}$ QC measured in the magnetic field $H = 5$ T with H parallel to (a) the threefold and fivefold axes, and (b) the twofold and fivefold axes (Matsuo et al., 1992).

The occurrence of diamagnetism in *i* Al–Cu–Fe QCs is not yet understood. It has been argued qualitatively (Cyrot-Lackmann, 1997) that diamagnetism is the consequence of very low electron effective masses in some directions for electron pockets of the Fermi sphere. This explanation has been questioned by Velikov et al. (2005b) who argued that

diamagnetism is due to the atomic-like diamagnetic contribution of tightly bound electrons in the electron pockets of the multiconnected Fermi surface.

In the Al–Cr–Fe system, magnetic properties of three alloys, polygrain *i* $Al_{86}Cr_8Fe_6$ (Stadnik and Müller, 1995; Stadnik et al., 1993), polygrain AP to both *i* and *d* QCs $Al_{61.3}Cr_{31.1}Fe_{7.6}$ (Bihar et al., 2006), and single-grain AP to a *d* QC $Al_{80}Cr_{15}Fe_5$ (Dolinšek et al., 2008a) were investigated. They are all paramagnets. Their $\chi(T)$ data were fitted to the modified Curie–Weiss law:

$$\chi = \chi_0 + \frac{C}{T-\theta}, \tag{1}$$

where χ_0 is the temperature-independent magnetic susceptibility, C is the Curie constant, and θ is the paramagnetic Curie temperature. The Curie constant can be expressed as $C = N\mu_{\text{eff}}^2/3k_B$, where N is the concentration of magnetic atoms per unit mass, μ_{eff} is the effective magnetic moment, and k_B is the Boltzmann constant. Table 2.1 lists the Curie–Weiss law parameters for these three alloys. Whereas similar negative values of θ are found for these three alloys, the values of χ_0 and μ_{eff} are significantly smaller for the *i* QC than for the other two APs. It was argued (Stadnik and Müller, 1995) that the origin of the nonzero μ_{eff} in the *i* $Al_{86}Cr_8Fe_6$ QC is due to disorder present in this metastable *i* QC. It was estimated (Bihar et al., 2006) that in the $Al_{61.3}Cr_{31.1}Fe_{7.6}$ AP, assuming that Cr does not carry a magnetic moment, only 2% of Fe atoms carry a magnetic moment of 6.2 μ_B.

Table 2.1 Parameters obtained from the fits of the $\chi(T)$ data to the modified Curie–Weiss law for three Al–Cr–Fe alloys

Alloy	X_0 (10^{-3} emu/mol)	C (10^{-3} emu K/mol)	θ (K)	$\mu_{\text{eff}}^{\text{TM}}(\mu_B)$	$\mu_{\text{eff}}^{\text{Fe}}(\mu_B)$	References
$Al_{86}Cr_8Fe_6$	2.60(1)	15.9(4)	−3.1 (2)	0.095 (1)	0.145 (2)	Stadnik and Müller (1995)
$Al_{61.3}Cr_{31.1}Fe_{7.6}$	20	720	−2	0.39	0.87	Bihar et al. (2006)
$Al_{80}Cr_{15}Fe_5$	4.5[a]	70.8	−6.0	0.17	0.34	Dolinšek et al. (2008a)
	5.5[b]	116	−4.5	0.22	0.43	
	6.1[c]	135	−5.4	0.23	0.46	

The symbols $\mu_{\text{eff}}^{\text{TM}}$ and $\mu_{\text{eff}}^{\text{Fe}}$ correspond, respectively, to the effective magnetic moment per TM (i.e., per Fe and Cr) and per Fe.
[a]Along the *a*-axis.
[b]Along the *b*-axis.
[c]Along the *c*-axis.

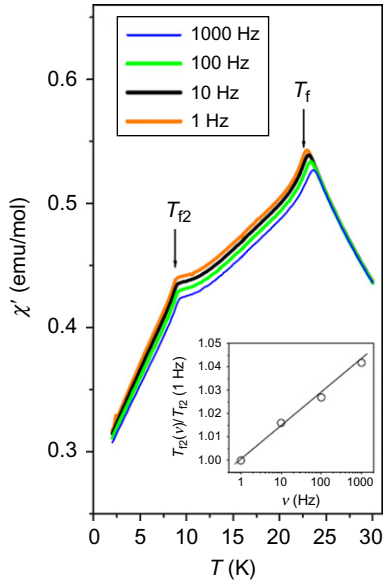

Figure 2.3 The temperature dependence of the ac susceptibility of the polygrain *d* $Al_{73}Mn_{21}Fe_6$ QC measured at different frequencies in a 6.5-Oe ac magnetic field. The inset shows the frequency dependence of $T_{f2}(\nu)/T_{f2}(1\ \text{Hz})$ (Dolinšek et al., 2008b).

The magnetic properties of the polygrain *d* $Al_{73}Mn_{21}Fe_6$ QC were studied by Dolinšek et al. (2008b). A clear bifurcation between the zero-field cooled (ZFC) and field-cooled (FC) $\chi(T)$ data at $T_f = 22.3$ K indicates the spin-glass nature of this QC. Surprisingly, another anomaly in the ZFC and FC $\chi(T)$ data was observed at $T_{f2} \approx 9$ K. The fit of the $\chi(T)$ data above T_f to Eq. (1) (assuming $\chi_0 = 0$) yielded $\theta = -23$ K and $\mu_{\text{eff}}^{\text{TM}} = 2.6\mu_B$. The ac susceptibility measurements (Fig. 2.3) clearly demonstrate the frequency-dependent shifts of T_f and T_{f2} (the values of K, the relative change in the freezing temperature per decade change in frequency ν, defined as $K = \Delta T_f / T_f \Delta \log \nu$, are equal to, respectively, 0.010 and 0.014). The spin-glass nature of the *d* $Al_{73}Mn_{21}Fe_6$ QC was further confirmed by observing (Dolinšek et al., 2008b) aging effects via thermoremanent magnetization (TRM) time decays for different aging (waiting) times t_w and cooling magnetic fields.

3.2. Al–Pd–Mn

Among all known QCs, the *i* Al–Pd–Mn QCs and their APs have been studied most extensively. It should be indicated first that the magnetic properties of single-phase, Bridgman-, Czochralski-, and flux-grown

single-grain or polygrain Al–Pd–Mn QCs are strongly sample dependent (Hippert et al., 2003; Swenson et al., 2004). This is illustrated in Fig. 2.4, which shows the $\chi(T)$ dependence for two polygrain and eight single-grain *i* Al–Pd–Mn QCs. The magnitude of χ varies by a factor of 55 between the E-a_1 and B-a_2 samples (Hippert et al., 2003).

The most thorough analysis of the magnetic data of many single-grain and polygrain *i* Al–Pd–Mn QCs was carried out by Hippert et al. (2003) and Préjean et al. (2006). One characteristic of the *i* Al–Pd–Mn QCs is that they are spin glasses with freezing temperature T_f in the range 0.23–3.6 K (Figs. 2.5–2.7).

The fits of the $\chi(T)$ data to the Curie–Weiss law result in very small values of *C*. Assuming that the Mn atoms carry a magnetic moment of 5.92 μ_B, the smallness of *C* implies that only a tiny fraction of Mn atoms, *f*, in *i* Al–Pd–Mn QCs (*f* is between a few percent down to about 10^{-4}) carry this magnetic moment (Hippert and Préjean, 2008). It has been argued

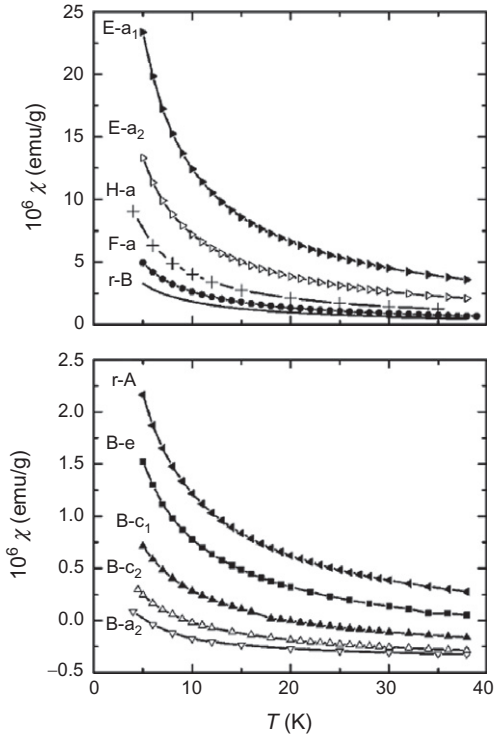

Figure 2.4 The temperature dependence of the magnetic susceptibility of two polygrain and eight single-grain *i* Al–Pd–Mn QCs measured in an external magnetic field of 1 kOe. Solid lines are guides to the eye (Hippert et al., 2003).

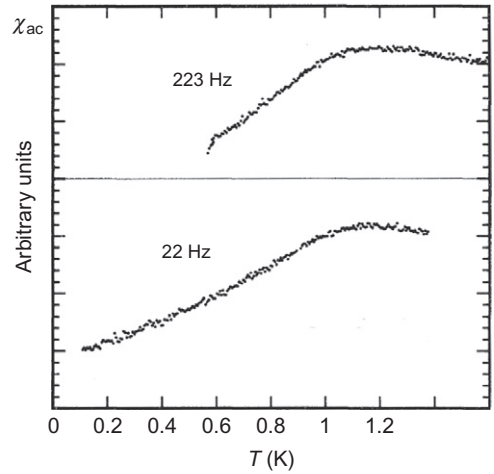

Figure 2.5 The temperature dependence of the ac susceptibility of the single-grain *i* $Al_{68.7}Pd_{21.5}Mn_{9.6}$ QC measured at two frequencies in a 1-Oe ac magnetic field (Lasjaunias et al., 1995).

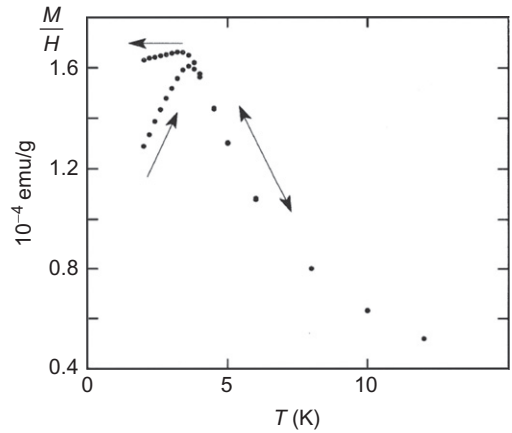

Figure 2.6 The temperature dependence of the ZFC and FC magnetic susceptibility of the polygrain *i* $Al_{71}Pd_{18}Mn_{11}$ QC measured in an external magnetic field of 8.6 Oe (Lasjaunias et al., 1995).

(Hippert and Préjean, 2008) that the reason for most Mn atoms being nonmagnetic is the presence of a pseudogap at the Fermi level that is predicted theoretically (Hafner and Krajčí, 1998; Hippert et al., 1999; Krajčí and Hafner, 1998) and observed experimentally (Escudero et al., 1999; Stadnik et al., 2001). It has been speculated (Hippert and Préjean, 2008) that the magnetic moment carried by a tiny fraction of the Mn atoms

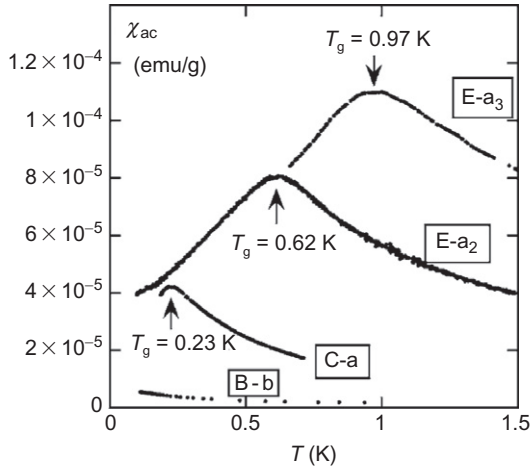

Figure 2.7 The temperature dependence of the ac susceptibility of four single-grain *i* Al–Pd–Mn samples (the sample compositions are given in Hippert et al. (2003)) measured in a 1-Oe ac magnetic field at the frequency of 1 Hz (Préjean et al., 2006).

is the consequence of the presence of local defects in the *i* structure of the Al–Pd–Mn QCs.

When one plots the measured χ versus $1/T$ for different *i* Al–Pd–Mn samples (Fig. 2.8), one notices a continuous change in the $\chi(1/T)$ dependence from a linear one for more magnetic samples (with a relatively large fraction of magnetic moment-carrying Mn atoms) to a nonlinear one for less magnetic samples. The nonlinear $\chi(1/T)$ dependence was interpreted as evidence of the presence of the Kondo effect (Hippert and Préjean, 2008; Préjean et al., 2006). Thus, the evolution of the $\chi(1/T)$ dependence indicates that in the magnetically strongest sample (sample R), there is a pure RKKY interaction, whereas in the magnetically weakest sample (sample B-b), there is a pure Kondo interaction; in the other samples, these two interactions coexist.

The magnetic properties of the polygrain *d* $Al_{69.8}Pd_{12.1}Mn_{18.1}$ QC were studied by Rau et al. (2003). This QC is a spin glass (Fig. 2.9) with $T_f = 12$ K. The fit of the $\chi(T)$ data above 120 K to Eq. (1) yields $\chi_0 = -2.45 \times 10^{-8}$ emu/g, $\theta = -20$ K, and $C = 0.544$ emu K/mol Mn. This value of C implies that $\mu_{eff} = 2.09\ \mu_B$ per Mn atom. Such a small value of μ_{eff} indicates that not all Mn atoms carry a magnetic moment. Assuming the paramagnetic moment of 5.92 μ_B for Mn^{3+}, this value of μ_{eff} implies that $f = 12.5\%$. Thus, similar to the situation for *i* Al–Pd–Mn QCs, only a small fraction of Mn atoms in the *d* Al–Pd–Mn QC carry a magnetic moment.

Hippert et al. (1999) studied the magnetic properties of five Al–Pd–Mn (Si) APs to the *i* and *d* Al–Pd–Mn QCs: polygrain 1/1 AP $Al_{68}Pd_{11}Mn_{14}Si_7$

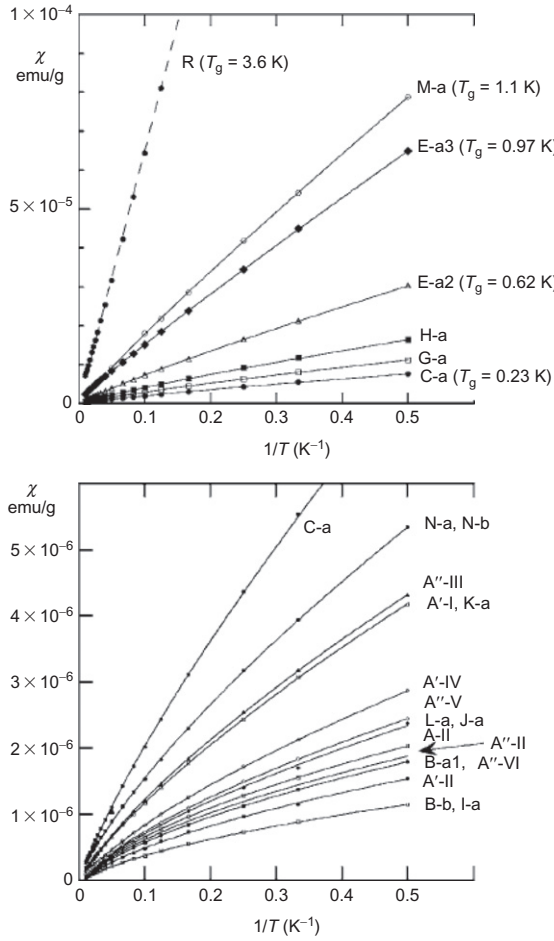

Figure 2.8 The magnetic susceptibility versus $1/T$ for 19 *i* Al–Pd–Mn samples. The solid lines are the Kondo fits in the framework of the one T_K model (Préjean et al., 2006).

(Fig. 2.10), polygrain 2/1 AP $Al_{70}Pd_{24}Mn_6$ (Fig. 2.11), single-grain, ξ'-phase, AP $Al_{71.9}Pd_{23.5}Mn_{4.6}$ (Fig. 2.11) (very similar $\chi(T)$ data for the single-grain ξ'-phase $Al_{72}Pd_{25}Mn_3$ were obtained later by Swenson et al., 2004), and two polygrain APs to the *d* QC, $Al_{73.1}Pd_{5.2}Mn_{21.7}$ and $Al_{78.5}Pd_{4.9}Mn_{16.6}$; the last two APs contained a small amount of foreign phases. The parameters derived from the fits of the $\chi(T)$ data to Eq. (1) for these five APs are given in Table 2.2. Hippert et al. (1999) argued that the increase in M/H below 30 K and the fact that the maximum of χ_{ac} is larger than the demagnetization factor of $3/4\pi$ for a spherical sample indicate that

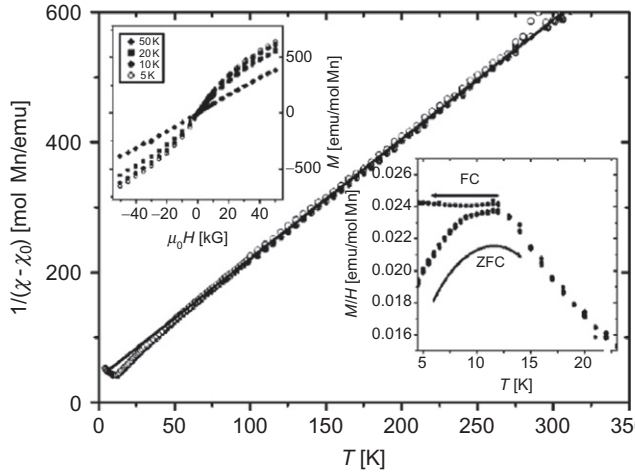

Figure 2.9 The inverse magnetic susceptibility corrected for the contribution χ_0, $(\chi - \chi_0)^{-1}$, versus temperature T for the d $Al_{69.8}Pd_{12.1}Mn_{18.1}$ QC measured in an external magnetic field of 500 Oe. The solid line is the fit to Eq. (1). The lower inset shows the temperature dependence of the ZFC and FC susceptibility. The upper inset displays the field dependence of the magnetization measured at several temperatures (Rau et al., 2003).

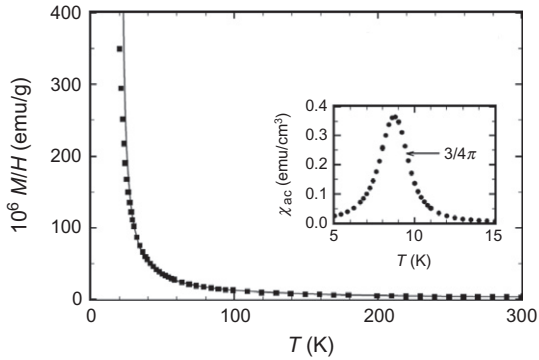

Figure 2.10 The temperature dependence of the dc magnetic susceptibility M/H measured in a magnetic field of 1 kOe for the 1/1 AP $Al_{68}Pd_{11}Mn_{14}Si_7$. The solid line is the fit to Eq. (1). The inset shows the temperature dependence of the ac magnetic susceptibility measured in a 1-Oe ac magnetic field at 13 Hz; the value of the demagnetization factor $(3/4\pi)$ for a spherical sample is indicated (Hippert et al., 1999).

the ferromagnetism with $T_c = 8.8$ K is not due to secondary phases but is probably an intrinsic property of this AP. The C values for the $Al_{70}Pd_{24}Mn_6$ and $Al_{71.9}Pd_{23.5}Mn_{4.6}$ APs (Table 2.2) imply very small values of f, 3×10^{-4} and 1.6×10^{-4}, respectively. Therefore, Hippert et al. (1999) considered

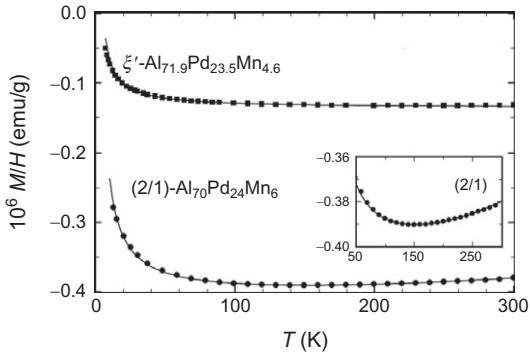

Figure 2.11 The temperature dependence of the dc magnetic susceptibility M/H measured in a magnetic field of 10 kOe for the 2/1 AP $Al_{70}Pd_{24}Mn_6$ and the ξ'-phase AP $Al_{71.9}Pd_{23.5}Mn_{4.6}$. The inset shows the M/H data above 50 K. The solid lines are the fits as explained in Table 2.2 caption (Hippert et al., 1999).

Table 2.2 Parameters obtained from the fits of the $\chi(T)$ data in the temperature ranges indicated in the second column to Eq. (1) for five Al–Pd–Mn(Si) alloys (with θ fixed to o for the second and third alloys)

Alloy	T range (K)	X_0 (10^{-6} emu/g)	C (10^{-6} emu K/g)
$Al_{68}Pd_{11}Mn_{14}Si_7$	30–300	0	1030
$Al_{70}Pd_{24}Mn_6$	5–300	−0.407	1.7
$Al_{71.9}Pd_{23.5}Mn_{4.6}$	5–300	−0.136	0.7
$Al_{73.1}Pd_{5.2}Mn_{21.7}$	30–100	5.0	1660
	150–300	0.8	2150
$Al_{78.5}Pd_{4.9}Mn_{16.6}$	150–300	0.4	50

For the $Al_{70}Pd_{24}Mn_6$ alloy, a T^2 contribution had to be added to Eq. (1) (Hippert et al., 1999).

these two APs to be nonmagnetic. The C values for the d AP $Al_{73.1}Pd_{5.2}Mn_{21.7}$ for the two temperature ranges (Table 2.2) correspond to the f values of 6.5% and 8.4%, respectively. The ZFC and FC $\chi(T)$ measurements, as well as the thermoremanent and isothermal remanent magnetization measurements, allowed one to establish that the $Al_{73.1}Pd_{5.2}Mn_{21.7}$ AP is a spin glass with $T_f \approx 14$ K (Hippert et al., 1999). As the C value for the $Al_{78.5}Pd_{4.9}Mn_{16.6}$ AP is about 40 times smaller than that for the $Al_{73.1}Pd_{5.2}Mn_{21.7}$ AP (Table 2.2), the $Al_{78.5}Pd_{4.9}Mn_{16.6}$ AP was considered to be nonmagnetic (Hippert et al., 1999).

It can be concluded that the magnetic properties of the Al–Pd–Mn QCs and their corresponding APs are quite similar to each other. In other words, quasiperiodicity does not seem to induce in the Al–Pd–Mn system any specific and unique magnetic characteristics that are not present in the corresponding periodic Al–Pd–Mn APs.

3.3. Al–TM–Co

In this system, two *d* QCs of high structural quality are known: *d* Al–Cu–Co and *d* Al–Ni–Co. It was first reported that the *d* $Al_{65}Cu_{15}Co_{20}$ QC is a diamagnet with the magnetic susceptibility of about -1×10^{-7} emu/g in the temperature range 10–300 K (Martin et al., 1991). Kimura et al. (1991) indicated that for the single-grain *d* $Al_{62}Cu_{20}Co_{15}Si_3$ QC, the values of χ are -2×10^{-7} and -4×10^{-7} emu/g measured along the quasiperiodic plane and the periodic axis, respectively. For the *d* $Al_{62}Cu_{20-}Co_{15}Si_3$ QC, the value of χ increases with temperature above 300 K (Lück and Kek, 1993).

The *d* $Al_{72}Ni_{12}Co_{16}$ QC is also a diamagnet (Fig. 2.12). Similar to what was observed for the *d* Al–Cu–Co QC, its magnetic susceptibility is strongly anisotropic.

The magnetic properties of the single-grain $Al_{76}Ni_{22}Co_2$ alloy of monoclinic structure, which is an AP to a *d* Al–Co–Ni QC, were studied by Smontara et al. (2008). The $\chi(T)$ data measured along the crystallographic directions [001] (designated as *c*), [010] (designated as *b*), and along the direction perpendicular to the (*a*,*b*) plane (designated as *a**) and lying in the monoclinic plane (the monoclinic plane corresponds to a quasiperiodic plane in a *d* QC) are shown in Fig. 2.13. The $\chi(T)$ data were fitted to the equation $\chi = \chi_0 + (C/T - \theta) + A_2T^2 + A_4T^4$ in which the terms A_iT_i ($i = 2,4$) were associated with the temperature-dependent susceptibility of conduction electrons (Smontara et al., 2008).

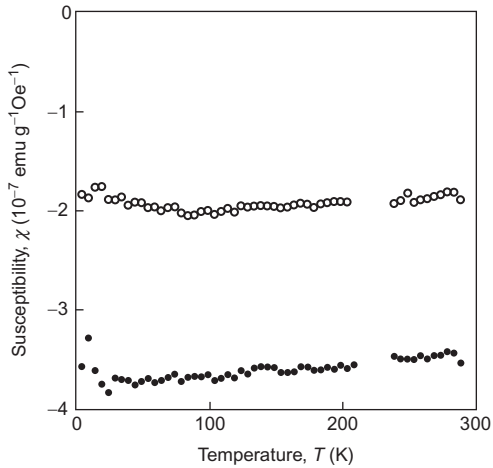

Figure 2.12 The temperature dependence of the magnetic susceptibility of the *d* $Al_{72}Ni_{12}Co_{16}$ QC measured along the periodic axis (open circles) and in the quasiperiodic plane (filled circles) (Yamada et al., 1999).

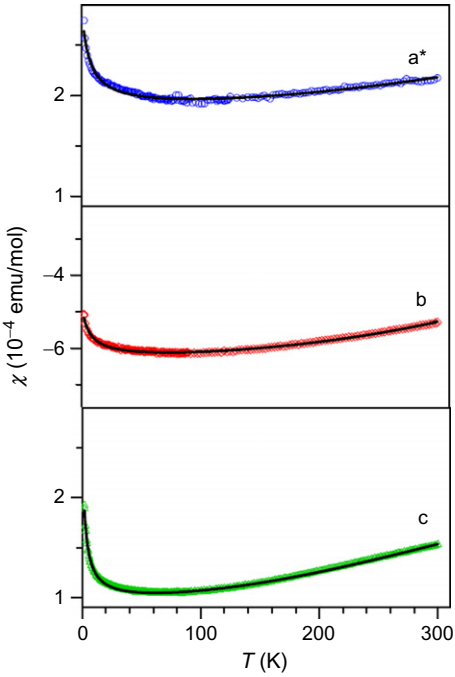

Figure 2.13 The temperature dependence of the magnetic susceptibility of $Al_{76}Ni_{22}Co_2$ measured in an external magnetic field of 10 kOe applied along three crystallographic directions (Smontara et al., 2008).

3.4. Al–TM–Ge

The *i* $Al_{65}Mn_{20}Ge_{15}$ QC was shown (Hundley et al., 1992) to be a spin glass with $T_f \approx 9$ K. The Mn atoms carry a relatively large magnetic moment of 2.1 μ_B.

Ferromagnetic behavior was reported in several Al–Mn–Ge QCs (Reisser and Kronmüller, 1994; Tsai et al., 1988) and Al–Cu–Mn–Ge QCs (Nasu et al., 1992; Reisser and Kronmüller, 1994). The presence of magnetically ordered second phase(s) in these QCs (Stadnik and Stroink, 1991) indicates that the observed ferromagnetism is probably of extrinsic origin.

The magnetic properties of the polygrain *d* $Al_{40}Mn_{25}Fe_{15}Ge_{20}$ QC were studied by Yokoyama et al. (1997) and Tobo et al. (2001). The ZFC and FC $\chi(T)$ data in different external magnetic fields and the ac $\chi'(T)$ data at different frequencies (Fig. 2.14) clearly demonstrate the spin-glass nature of this QC with $T_f \approx 41$ K.

3.5. Al–Pd–TM–B

The ferromagnetic order in the polygrain *i* $Al_{70-x}Pd_{15}Mn_{15}B_x$ QCs with $x \geq 3$ was reported by Yokoyama et al. (1994) and Peng et al. (1998). The curves of magnetization M versus external magnetic field H (Figs. 2.15 and 2.16) are characteristic of a ferromagnet with the Mn magnetic moment in

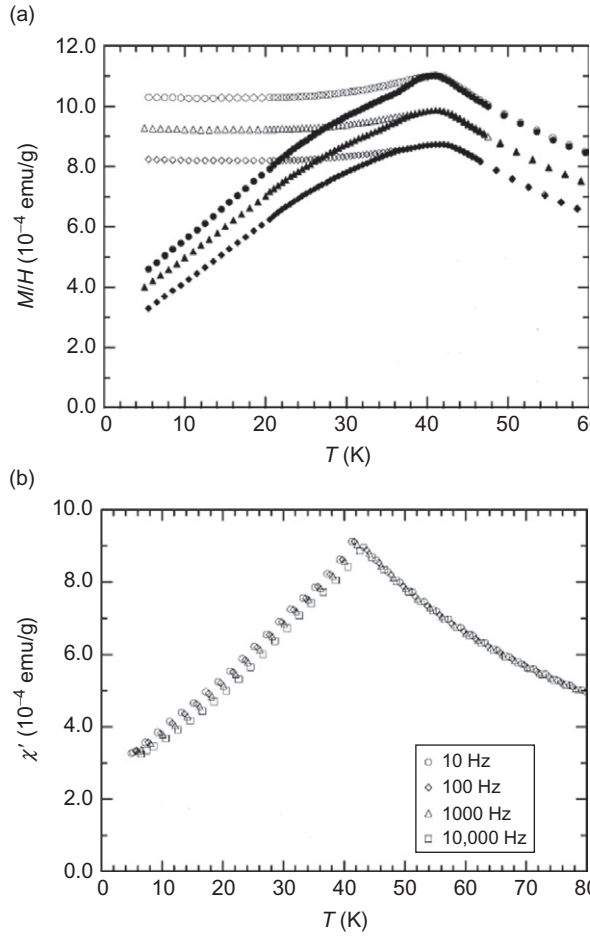

Figure 2.14 (a) The temperature dependence of the ZFC (filled symbols) and FC (open symbols) magnetic susceptibility of the polygrain *d* $Al_{40}Mn_{25}Fe_{15}Ge_{20}$ QC measured in an external magnetic field of 50 (circles), 100 (triangles), and 200 Oe (diamonds). The M/H curves measured in the fields of 50 and 100 Oe are shifted upward to avoid overlap. (b) The temperature dependence of the in-phase magnetic susceptibility χ' of the polygrain *d* $Al_{40}Mn_{25}Fe_{15}Ge_{20}$ QC measured in a 10-Oe ac magnetic field at different frequencies (Tobo et al., 2001).

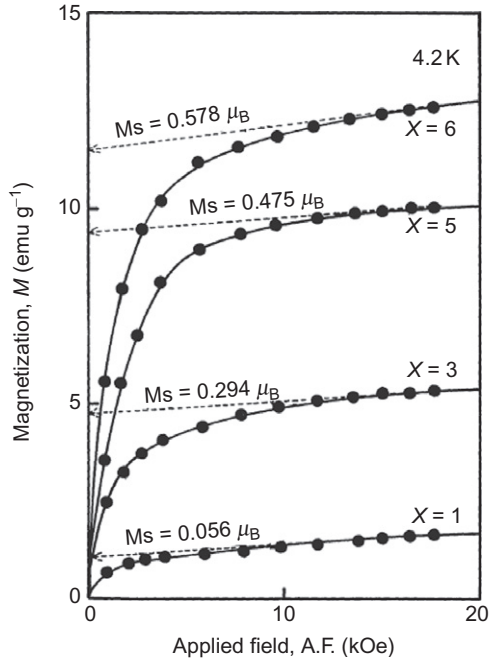

Figure 2.15 The magnetization versus the external magnetic field at 4.2 K for the *i* $Al_{70-x}Pd_{15}Mn_{15}B_x$ QCs (Yokoyama et al., 1994).

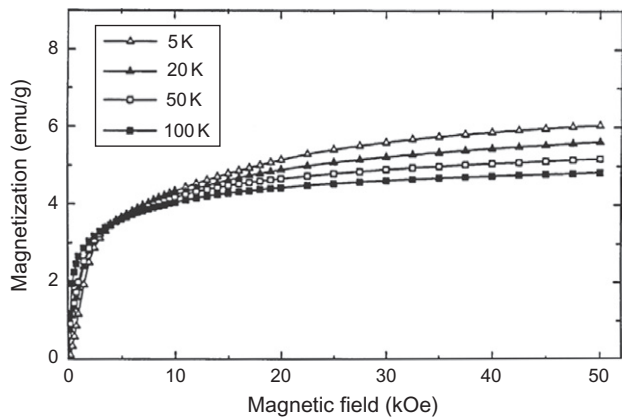

Figure 2.16 The magnetization versus the external magnetic field at different temperatures for the *i* $Al_{65.5}Pd_{15}Mn_{15}B_{4.5}$ QC (Peng et al., 1998).

the range 0.3–0.6 μ_B. The Curie temperatures T_C of these ferromagnets were found to be above 500 K (Fig. 2.17), although in another study (Bahadur et al., 1995), they were determined to be below 500 K. No presence of second phases could be seen in the X-ray and electron diffraction patterns of

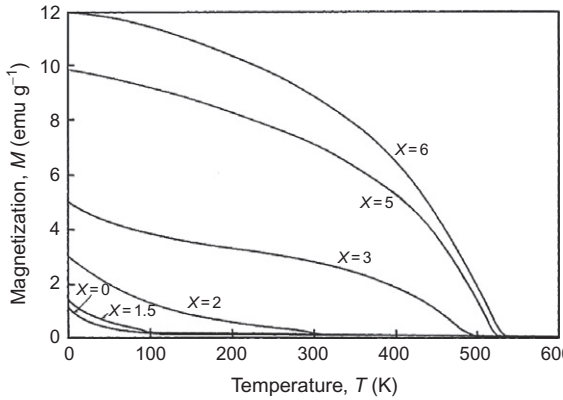

Figure 2.17 The temperature dependence of the magnetization of the *i* $Al_{70-x}Pd_{15}Mn_{15}B_x$ QCs measured in an external magnetic field of 10 kOe (Yokoyama et al., 1994).

these QCs (Yokoyama et al., 1994); however, it should be noted that MnB, a possible impurity phase, is a strong ferromagnet with $T_C = 572$ K (Beckman and Lundgren, 1991). To assert that ferromagnetism of these QCs is of intrinsic origin, neutron diffraction experiments would be very desirable.

Inhomogeneous ferromagnetism was claimed to occur in the polygrain *i* $Al_{70-x}Pd_{30-y}B_xFe_y$ QCs with the T_c values in the range 280–340 K (Lin et al., 1995a; Lyubutin et al., 1997). The low-resolution X-ray diffraction spectra of these QCs do not exclude the possibility of the presence of magnetic crystalline/amorphous impurities. Neutron diffraction studies of these QCs are needed to verify the possible ferromagnetic quasiperiodic order.

3.6. Al–Pd–Mn–Ge, Al–TM–Ge–B

Spin-glass behavior was observed for the *i* $Al_{70-x}Pd_{12.5}Mn_{17.5}Ge_x$ QCs with $x \leq 6$ (Lin et al., 1995b). The QCs with $x > 6$ contained a significant amount of magnetically ordered impurities. Ferromagnetic order was reported in the *d* $Al_{25}Mn_{45-x}Ge_{15}B_{15}Fe_x$ QCs (Yokoyama and Inoue, 1996a,b). The X-ray diffraction spectra of these QCs indicate the presence of crystalline impurities. The reported ferromagnetism is probably of an extrinsic nature.

4. QCs and APs Not Based on Al

4.1. Zn–Mg–RE

The discovery of thermodynamically stable, highly ordered *i* QCs in the Zn–Mg–RE (rare earth) system (Niikura et al. 1994; Tsai et al., 1994) led to intensive studies of their magnetic properties as RE atoms are expected to

carry localized magnetic moments and, perhaps, this could result in a long-range quasiperiodic magnetic order in these QCs. They have a face-centered (or F type) 6D Bravais lattice. The early magnetic measurements were carried out on polygrain samples. It was soon demonstrated that high-quality, single-grain *i* Zn–Mg–RE QCs (Fig. 2.18) could be synthesized (Fisher et al., 1998; Sato et al., 1998a). It turns out that the *i* Zn–Mg–RE QCs are spin glasses. The occurrence of a bifurcation between the ZFC and FC $\chi(T)$ data, a hallmark of a spin glass (Mydosh, 1993), is evident (Fig. 2.19). The parameters obtained from the fit of the $\chi(T)$ data above T_f to the modified Curie–Weiss law for polygrain and single-grain *i* Zn–Mg–RE QCs are given in Table 2.3. The negative values of θ indicate a predominantly antiferromagnetic interaction between the RE magnetic moments. They scale approximately with the de Gennes factor (Fisher et al., 1999; Hattori et al., 1995). It is clear that the values of $\mu_{\mathrm{eff}}^{\mathrm{RE}}$ are very close to the theoretical moments $\mu_{\mathrm{th}}^{\mathrm{RE}}$ for RE^{3+} free ions, which indicates that the RE magnetic moments are well localized with no significant crystalline-electric field effects.

The occurrence of spin-glass behavior requires both randomness and frustration (Binder and Young, 1986; Mydosh, 1993; Toulouse, 1977). The frustration parameter *f*, defined as $f = -\theta/T_f$ (Ramirez, 2001), is an empirical measure of frustration. Compounds with $f > 10$ are categorized as strongly geometrically frustrated compounds (Ramirez, 2001). The values of *f* for the *i* Zn–Mg–RE QCs (Table 2.3) are sufficiently large to allow one to conclude that frustration dominates the magnetic properties of these QCs.

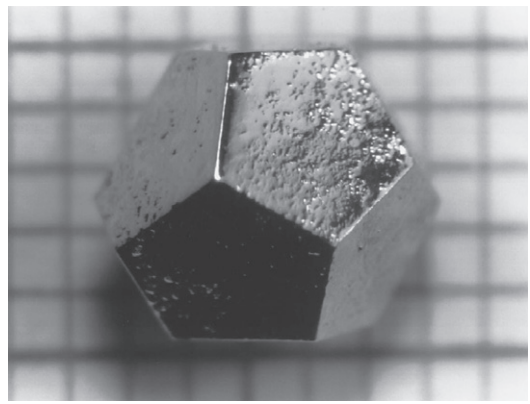

Figure 2.18 The photograph of a single-grain *i* $Zn_{56.8}Mg_{34.6}Ho_{8.7}$ QC shown over a mm scale. The clearly defined pentagonal facets and the dodecahedral morphology are visible (Fisher et al., 1999).

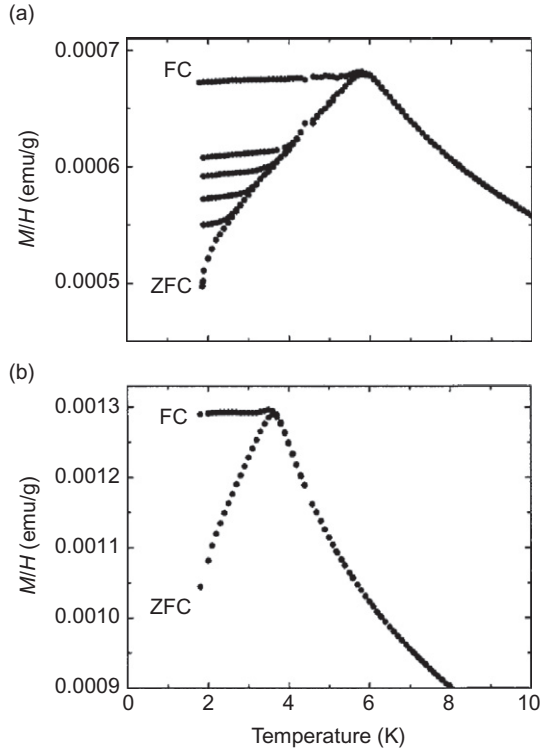

Figure 2.19 The temperature dependence of the ZFC and FC magnetic susceptibility of the single-grain *i* QCs $Zn_{56.8}Mg_{34.6}Tb_{8.7}$ QC (a) and $Zn_{56.8}Mg_{34.6}Dy_{8.7}$ (b) measured in an external magnetic field of 25 Oe. Also shown in (a) are FC data for field cooling from 2.5, 3.0, 3.5, and 4.0 K (Fisher et al., 1999).

Figure 2.20 shows the temperature dependence of the in-phase component χ' and the out-of-phase component χ'' of the ac magnetic susceptibility of the single-grain *i* $Zn_{56.8}Mg_{34.6}Tb_{8.7}$ QC for different frequencies. Both $\chi'(T)$ and $\chi''(T)$ curves show maxima whose amplitudes and positions depend on the frequency f of the applied ac magnetic field. With increasing f, the peak positions are shifted to higher temperatures, the peak intensity of $\chi'(T)$ decreases, and the peak intensity of $\chi''(T)$ increases. These features are typical of canonical spin glasses (Mydosh, 1993). The position of the sharp peak in $\chi'(T)$ can be used to define T_f. The observed change of T_f with f (Fig. 2.20) corresponds to $K=0.049$, a value comparable to that of other canonical spin glasses. The frequency dependence of T_f was accounted for (Fisher et al., 1999) by the phenomenological Vogel–Fulcher law:

$$f = f_0 \exp\left[-\frac{E_a}{k_B(T_f - T_0)}\right], \tag{2}$$

Table 2.3 Parameters obtained from the fits of the $\chi(T)$ data to the modified Curie–Weiss law for the polygrain (Charrier and Schmitt, 1997; Hattori et al., 1995; Kashimito et al., 1999) and single-grain (Fisher et al., 1999) *i* Zn–Mg–RE QCs

Alloy	θ (K)	$\mu_{\mathrm{eff}}^{\mathrm{RE}}(\mu_{\mathrm{B}})$	$\mu_{\mathrm{th}}^{\mathrm{RE}}(\mu_{\mathrm{B}})$	T_{f} (K)	References
$Zn_{50}Mg_{42}Gd_8$	−38	7.95	7.94	5.5	Hattori et al. (1995)
$Zn_{50}Mg_{42}Tb_8$	−24	10.29	9.72	7.6	Hattori et al. (1995)
	−26	10.05		5.8	Charrier and Schmitt (1997)
$Zn_{56.8}Mg_{34.6}Tb_{8.7}$	−26.3(4)	9.91(3)		5.80(5)	Fisher et al. (1999)
$Zn_{50}Mg_{42}Dy_8$	−14	10.83	10.65		Hattori et al. (1995)
	−17.2	9.78		3.8	Charrier and Schmitt (1997)
$Zn_{56.8}Mg_{34.6}Dy_{8.7}$	−14.8(4)	10.50 (3)		3.60(5)	Fisher et al. (1999)
$Zn_{50}Mg_{42}Ho_8$	−8	10.08	10.61		Hattori et al. (1995)
	−10	9.79		∼2	Charrier and Schmitt (1997)
$Zn_{60}Mg_{30}Ho_{10}$	−8.97	10.6			Kashimito et al. (1999)
$Zn_{56.8}Mg_{34.6}Ho_{8.7}$	−7.8(4)	10.36 (3)		1.95(5)	Fisher et al. (1999)
$Zn_{50}Mg_{42}Er_8$	−5	8.88	9.58		Hattori et al. (1995)
	−6.3	9.59		<1.5	Charrier and Schmitt (1997)
$Zn_{56.8}Mg_{34.6}Er_{8.7}$	−5.1(4)	9.49(3)		1.30(5)	Fisher et al. (1999)

where f_0 is the characteristic frequency, E_a is the activation energy, and T_0 is the Vogel–Fulcher temperature, which is a measure of the strength of interaction between clusters in the spin glass. The best fit of the $T_f(f)$ data (Fig. 2.20) to Eq. (2) yielded $f_0 = 4(1) \times 10^7$ Hz, $E_a/k_B = 27(1)$ K, and $T_0 = 4.8(1)$ K. The obtained values of these three parameters are in general agreement with similar parameters reported for other spin glasses.

The most convincing way to demonstrate the spin-glass nature of a given compound is to measure the temperature dependence of the nonlinear, third-order (fifth-order, etc.) magnetic susceptibility χ_3 as it is expected to diverge negatively at T_f (Lévy, 1988). As it is shown in Fig. 2.21, such a divergence is clearly observed for the *i* $Zn_{56.8}Mg_{34.6}Tb_{8.7}$ and $Zn_{56.8}Mg_{34.6}Ho_{8.7}$ QCs.

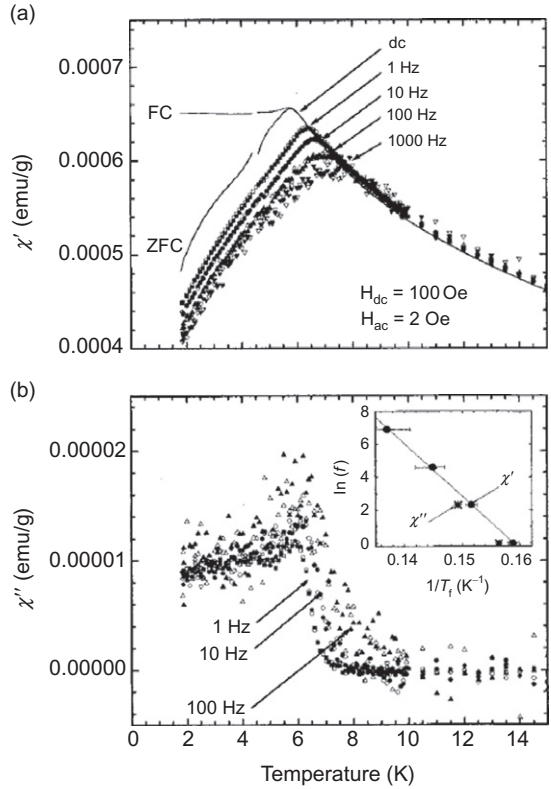

Figure 2.20 The temperature dependence of the in-phase magnetic susceptibility χ' (a) and out-of-phase magnetic susceptibility χ'' (b) measured in a steady bias field of 100 Oe and in a 2-Oe ac magnetic field for different applied frequencies for the *i* $Zn_{56.8}Mg_{34.6}Tb_{8.7}$ QC. The inset in (b) shows the ln(*f*) versus $1/T_f$ dependence with a linear fit (solid line) to the T_f data (Fisher et al., 1999).

An inherent characteristic of a spin-glass system is an aging phenomenon (Lundgren et al., 1983). It can be studied, for example, via a TRM time decay measurement (Mydosh, 1993) which involves cooling the sample in a small magnetic field from above T_f to the measuring temperature T_m below T_f, keeping the sample at T_m for a certain waiting time t_w, and then rapidly removing the magnetic field and recording the change in magnetization with time. Figure 2.22 shows such TRM decays for different waiting times for the single-grain *i* $Zn_{56.8}Mg_{34.6}Tb_{8.7}$ QC (Dolinšek et al., 2001). One can clearly observe that the TRM increases and its time decay slows down as t_w increases. The observed dependencies of the TRM and its decay rate upon t_w are precisely the same as those observed for canonical spin glasses and can be explained within the context of an ultrametric organization of

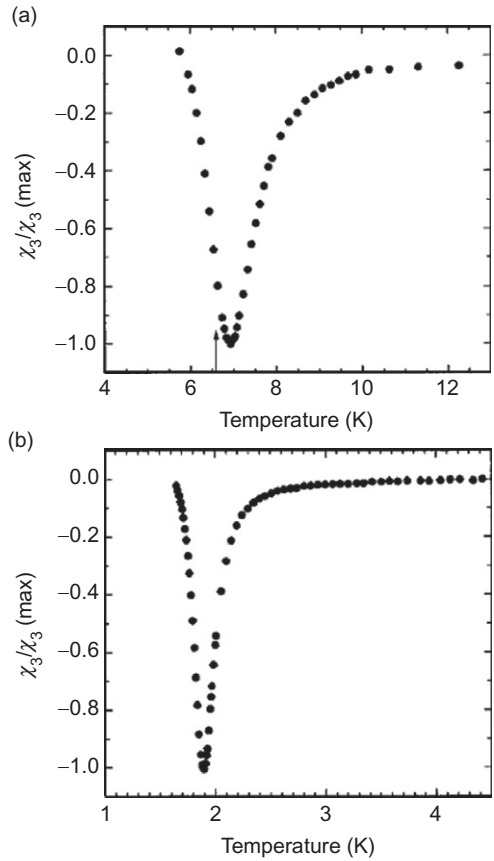

Figure 2.21 The temperature dependence of the third-order ac magnetic susceptibility χ_3 of (a) *i* $Zn_{56.8}Mg_{34.6}Tb_{8.7}$ QC (at 7 Hz) and (b) *i* $Zn_{56.8}Mg_{34.6}Ho_{8.7}$ QC (at 21 Hz), normalized by the maximum value χ_3(max). A vertical error in (a) indicates T_f for a measurement frequency of 7 Hz, estimated from the χ' data in Fig. 2.20 (Fisher et al., 1999).

the metastable states in a spin glass (Dolinšek et al., 2001, 2003). The dependence of the TRM on the magnetic field H_{fc} in which the sample was cooled H_{fc} for the single-grain *i* $Zn_{56.8}Mg_{34.6}Tb_{8.7}$ QC is shown in Fig. 2.23. A clear TRM increase is observed with H_{fc} . As argued qualitatively by Dolinšek et al. (2001, 2003), the TRM is expected to decrease with H_{fc} for the ultrametrically organized metastable states in a spin glass. Dolinšek et al. (2001, 2003) concluded that the observed dependence TRM (H_{fc}) is compatible with the *i* $Zn_{56.8}Mg_{34.6}Tb_{8.7}$ QC being a superparamagnet rather than a spin glass.

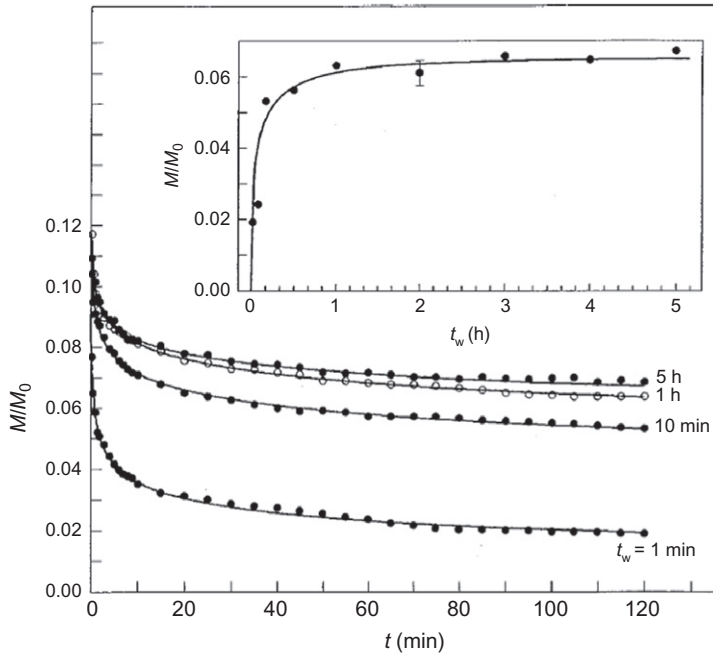

Figure 2.22 The TRM (magnetization M normalized to the FC value M_0) time decays at $H_{fc} = 125$ Oe for different waiting times t_w at 4.2 K for the *i* $Zn_{56.8}Mg_{34.6}Tb_{8.7}$ QC. The inset shows the values of M/M_0 recorded after the decay time of 120 min as a function of t_w (Dolinšek et al., 2001).

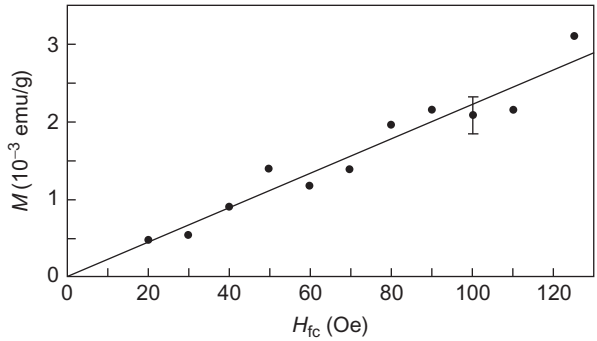

Figure 2.23 The dependence of the TRM recorded after the decay time $t = 120$ min at 4.2 K for $t_w = 1$ h on the field H_{fc} for the *i* $Zn_{56.8}Mg_{34.6}Tb_{8.7}$ QC (Dolinšek et al., 2001).

In the first neutron diffraction study of the polygrain *i* $Zn_{50}Mg_{42}RE_8$ (RE = Tb, Dy, Ho, Er) QCs, Charrier et al. (1997) observed rather weak magnetic Bragg reflections that were claimed to originate from the long-range quasiperiodic antiferromagnetic order (Fig. 2.24), coexisting with significant diffuse scattering (Fig. 2.25), both of which disappeared above the Néel temperatures T_N of 20, 12, 7, and 5 K for Tb, Dy, Ho, and Er QCs, respectively. Almost all the magnetic Bragg reflections could be indexed with a single propagation vector **Q** of $\left(\frac{1}{4},0,0,0,0,0\right)$ in the 6D reciprocal lattice (Fig. 2.24b), and this was taken as evidence for the long-range quasiperiodic antiferromagnetic order. Charrier et al. (1997) observed

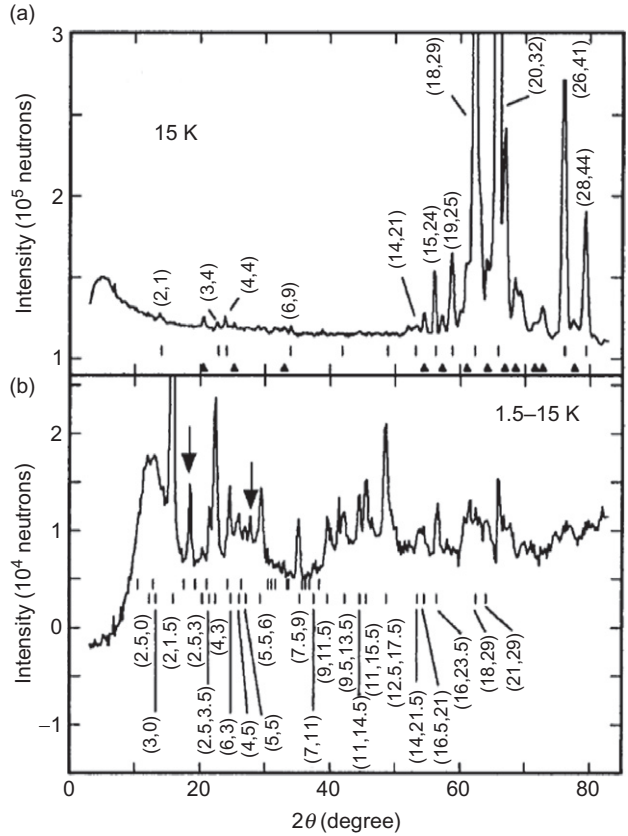

Figure 2.24 (a) The neutron diffraction pattern at 15 K for the *i* $Zn_{50}Mg_{42}Ho_8$ QC. The indices of the nuclear Bragg reflections are based on the indexing scheme of Cahn et al. (1986). The triangles indicate the reflections due to the impurity Mg_7Zn_3. (b) The difference between the patterns at 1.5 and 15 K. The magnetic indices are related to the nuclear indices via $(N_{mag},M_{mag}) = (N+0.125,M+0.0625)$. The arrows indicate the positions of the 2**Q** harmonics (Charrier et al., 1997).

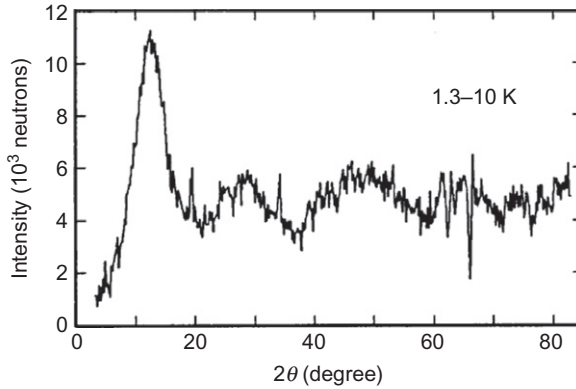

Figure 2.25 The difference between the neutron diffraction patterns at 1.3 and 10 K for the *i* $Zn_{50}Mg_{42}Er_8$ QC (Charrier et al., 1997).

clear magnetic reflections with weaker broad magnetic peaks due to diffuse scattering for the Tb and Dy QCs, and very weak magnetic reflections with very strong diffuse magnetic peaks for the Ho and Er QCs. Surprisingly, no anomaly at T_N could be seen in the $\chi(T)$ data (Charrier and Schmitt, 1997).

The claim that a long-range quasiperiodic antiferromagnetic order exists in *i* Zn–Mg–RE QCs was challenged by other researchers. Islam et al. (1998) carried out a neutron diffraction study of the single-grain *i* $Zn_{56.8}Mg_{34.6}Tb_{8.7}$ QC. Figure 2.26 shows the neutron diffraction patterns of this QC at 30 and 4 K and their difference. It is clear that apart from the onset of short-range magnetic order at low temperatures, there is no evidence for the presence of sharp magnetic Bragg reflections. Islam et al. (1998) also found that, for the polygrain *i* $Zn_{56.8}Mg_{34.6}Tb_{8.7}$ QC, the neutron diffraction patterns are similar to those in Fig. 2.26 and contain an impurity magnetic Bragg reflection which, together with the diffuse component, disappears above about 20 K, that is, above the apparent T_N of this QC. This indicates that the long-range antiferromagnetic order observed by Charrier et al. (1997) might be of extrinsic origin.

In another neutron diffraction study, Sato et al. (1998b) measured the spectra of the polygrain *i* $Zn_{60}Mg_{30}Tb_{10}$ QC at 20 and 1.6 K. As can be seen from Fig. 2.27a, the magnetic Bragg reflections are clearly absent and only the diffuse Bragg peaks are present at similar positions to those observed by Charrier et al. (1997). The magnetic Bragg reflections in the neutron diffraction spectrum of the hexagonal $(Zn_{0.8}Mg_{0.2})_5Ho$ alloy (Fig. 2.27b), which is an antiferromagnet with $T_N = 7.4$ K (Sato et al., 2000a), are located at the same positions as those in Fig. 2.24. This constitutes strong evidence that the claimed long-range antiferromagnetic order in the *i* $Zn_{50}Mg_{42}Ho_8$ QC with $T_N = 7$ K (Charrier et al., 1997) is due to the magnetic impurity $(Zn,Mg)_5Ho$.

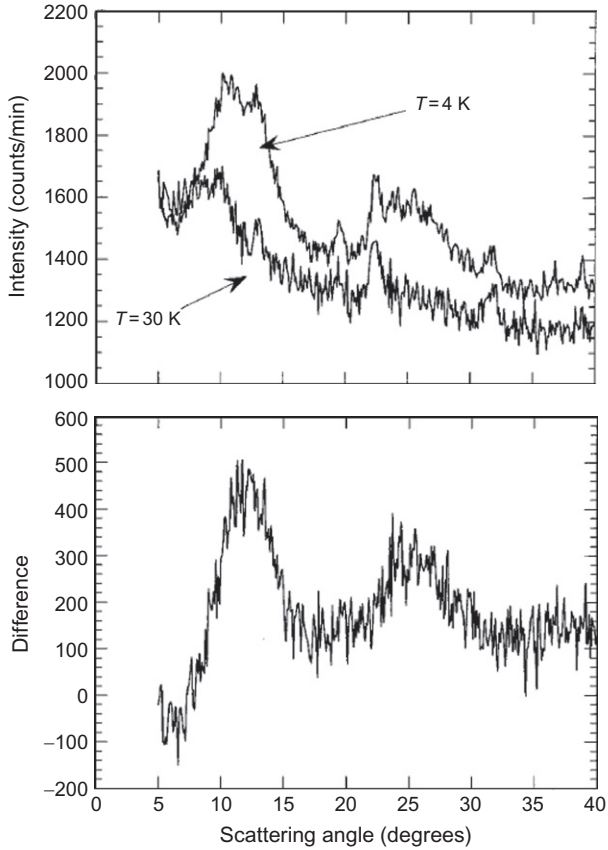

Figure 2.26 The top panel shows the neutron diffraction patterns at 4 and 30 K for the *i* $Zn_{56.8}Mg_{34.6}Tb_{8.7}$ QC. The lower panel shows the difference in pattern resulting from a subtraction $I(4\text{ K}) - I(30\text{ K})$ of the data from the top panel (Islam et al., 1998).

The nature of the short-range magnetic order and spin-glass-like freezing in *i* Zn–Mg–Ho(Tb) QCs was studied by inelastic neutron scattering (Sato, 2005; Sato et al., 2000b, 2006). Significant static short-range antiferromagnetic correlations were detected with a correlation length in the range 10–20 Å. Such a significant short-range order, which is not present in canonical spin glasses, points to the possible existence of a cluster with strongly coupled spins. It was conjectured that this cluster is in the form of a dodecahedron with spins at its vertices. It was demonstrated that the observed diffuse scattering patterns could be reasonably well accounted for by using this dodecahedral spin cluster model (Sato, 2005; Sato et al., 2006). The possible existence of dodecahedral spin clusters indicates that the *i* Zn–Mg–RE QCs are closer to superparamagnets than to spin glasses, which is a

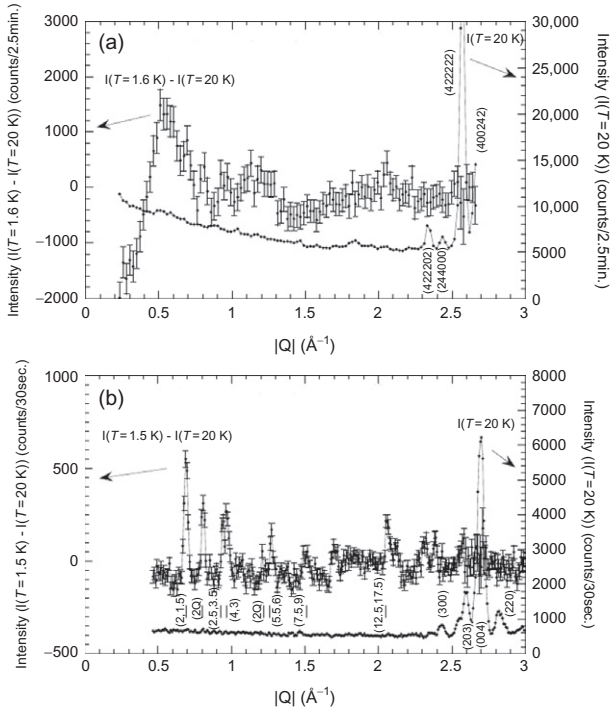

Figure 2.27 (a) The neutron diffraction pattern at 20 K and the difference between the neutron diffraction patterns at 1.6 and 20 K for the polygrain *i* $Zn_{60}Mg_{30}Tb_{10}$ QC. The indices of the nuclear Bragg reflections are based on the indexing scheme of Elser (1985). (b) The neutron diffraction pattern at 20 K and the difference between the neutron diffraction patterns at 1.5 and 20 K for the crystalline $(Zn_{0.8}Mg_{0.2})_5Ho$ alloy. The magnetic Bragg reflections of the difference spectrum are indexed in the same way as in Fig. 2.24 (Sato et al., 1998b).

conclusion drawn earlier from the TRM decay studies (Dolinšek et al., 2001, 2003). It was argued (Sato et al., 2006) that even though the cluster formation is essential to explaining the macroscopic freezing at T_f in the *i* Zn–Mg–RE QCs, this freezing is different from the blocking phenomenon in superparamagnets or the freezing in spin glasses; whereas it is the motion of the entire dodecahedral spin cluster, and not individual spins, that freezes at T_f in the *i* Zn–Mg–RE QCs, it is the individual spins that freeze in spin glasses or superparamagnets.

Magnetic properties of two pseudoternary single-grain *i* QCS, Zn–Mg–$(Y_{1-x}Tb_x)(0.075 \leq x \leq 0.88)$ and Zn–Mg–$(Y_{1-x}Gd_x)(0.075 \leq x \leq 0.60)$, were studied by Fisher et al. (1999). These QCs are spin glasses with T_f varying between 0.54 and 5.20 K.

4.2. Cd–Mg–RE

Discovered by Guo et al. (2000a), this is a second *i* system containing RE elements. In contrast to the *i* Zn–Mg–RE QCs, the *i* Cd–Mg–RE QCs have a primitive (or P type) 6D Bravais lattice. The fit of the $\chi^{-1}(T)$ data to Eq. (1) for temperatures above 50 K for the single-grain *i* $Cd_{50}Mg_{40}RE_{10}$ (Fig. 2.28) and the polygrain *i* $Cd_{55}Mg_{35}RE_{10}$ QCs (Sato et al., 2001) yield the parameters listed in Table 2.4. Similar to what was found for the *i* Zn–Mg–RE QCs (Table 2.3), negative values of θ (Table 2.4) indicate

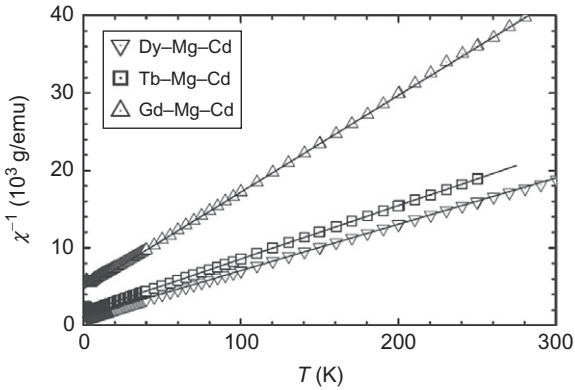

Figure 2.28 The inverse magnetic susceptibility versus temperature for the single-grain *i* $Cd_{50}Mg_{40}RE_{10}$ (RE = Dy, Tb, Gd) QCs measured in an external magnetic field of 1000 Oe. The solid lines are the fits to Eq. (1) assuming $\chi_0 = 0$ with parameters given in Table 2.4 (Sebastian et al., 2004).

Table 2.4 Parameters obtained from the fits of the $\chi(T)$ data to the modified Curie–Weiss law for the single-grain (Sebastian et al., 2004) and polygrain (Sato et al., 2001) *i* Cd–Mg–RE QCs

Alloy	θ (K)	$\mu_{eff}^{RE}(\mu_B)$	$\mu_{th}^{RE}(\mu_B)$	T_f (K)	T_{fl} (K)	References
$Cd_{50}Mg_{40}Gd_{10}$	−37.8 (1)	7.24	7.94	4.3(1)		Fisher et al. (2004)
$Cd_{55}Mg_{35}Gd_{10}$	−37	7.90		4.8	13.0	Sato et al. (2001)
$Cd_{50}Mg_{40}Tb_{10}$	−24.5 (1.5)	9.74	9.72	5.9(5)		Fisher et al. (2004)
$Cd_{55}Mg_{35}Tb_{10}$	−23	10.03		5.6	12.5	Sato et al. (2001)
$Cd_{50}Mg_{40}Dy_{10}$	−18.4 (1.0)	10.59	10.65	3.2(1)		Fisher et al. (2004)
$Cd_{55}Mg_{35}Dy_{10}$	−14	10.67		3.8	7.4	Sato et al. (2001)
$Cd_{55}Mg_{35}Ho_{10}$	−7	10.42	10.61	5.0	12.5	Sato et al. (2001)
$Cd_{55}Mg_{35}Er_{10}$	−6	9.71	9.58		4.4	Sato et al. (2001)
$Cd_{55}Mg_{35}Tm_{10}$	−2	7.08	7.56			Sato et al. (2001)

dominant antiferromagnetic interactions between the RE magnetic moments and they scale with the de Gennes factor (Sato et al., 2001; Sebastian et al., 2004). Also, the values of $\mu_{\text{eff}}^{\text{RE}}$ are close to the theoretical moments $\mu_{\text{th}}^{\text{RE}}$ for RE^{3+} free ions. This is indicative of the RE magnetic moments being well localized with no significant crystalline-electric field effects. The ZFC and FC $\chi(T)$ data for the single-grain *i* $Cd_{50}Mg_{40}RE_{10}$ (Fig. 2.29) and $Cd_{55}Mg_{35}Tb_{10}$ (Fig. 2.30) QCs indicate that these QCs are spin glasses. Surprisingly, two distinct freezing temperatures are observed for the polygrain Cd–Mg–RE QCs (Fig. 2.30), in contrast to the one freezing temperature observed for the single-grain Cd–Mg–RE QCs (Fig. 2.29). This observation is confirmed in the ac $\chi(T)$ data (Figs. 2.31 and 2.32). The values of T_f for the single-grain QCs correspond to the lower of the two freezing temperatures found for polygrain QCs (Table 2.4). This suggests that the double-freezing transition observed in polygrain samples is due to an impurity phase (Sebastian et al., 2004) that is not present in the single-grain samples.

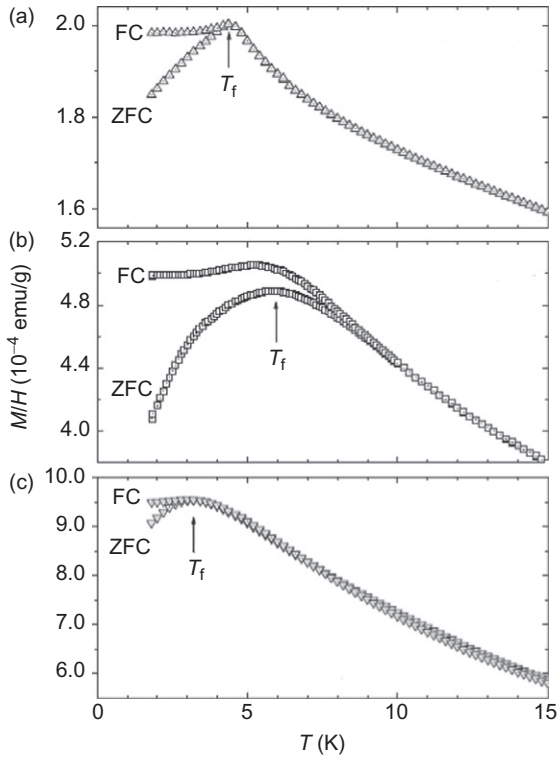

Figure 2.29 The temperature dependence of the ZFC and FC magnetic susceptibility of the single-grain *i* QCs $Cd_{50}Mg_{40}Gd_{10}$ (a), $Cd_{50}Mg_{40}Tb_{10}$ (b), and $Cd_{50}Mg_{40}Dy_{10}$ (c) measured in an external magnetic field of 100 Oe (Sebastian et al., 2004).

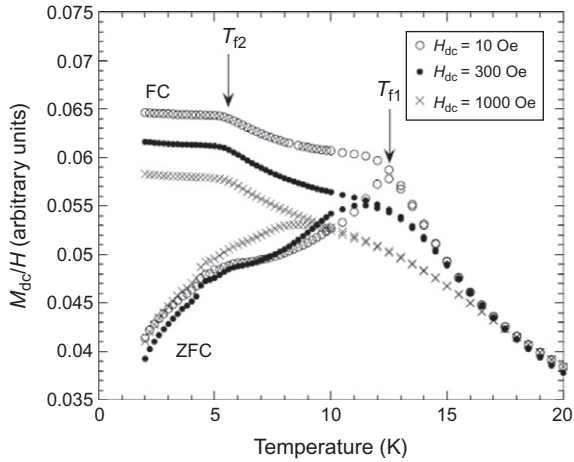

Figure 2.30 The temperature dependence of the ZFC and FC magnetic susceptibility of the polygrain *i* $Cd_{55}Mg_{35}Tb_{10}$ QC measured in different external magnetic fields. The arrows indicate the positions of the high (T_{f1}) and low (T_f) (Table 2.4) spin-freezing temperatures (Sato et al., 2001).

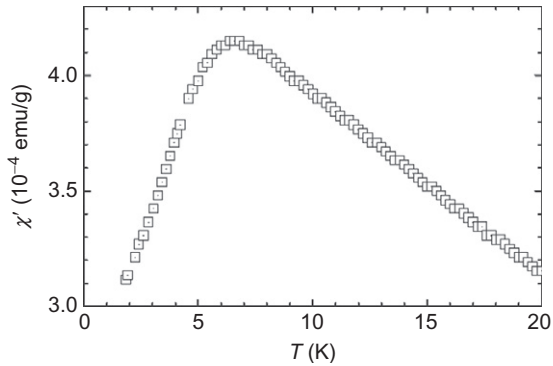

Figure 2.31 The temperature dependence of the ac susceptibility of the single-grain *i* $Cd_{50}Mg_{40}Tb_{10}$ QC measured at a frequency of 10 Hz in a steady bias field of 50 Oe and a 1-Oe ac magnetic field (Sebastian et al., 2004).

One finds that, for some of the Cd–Mg–RE QCs, the frustration parameter f is rather large (Table 2.4). They can thus be categorized as strongly geometrically frustrated magnets (Ramirez, 2001).

Neutron diffraction experiments carried out on the polygrain *i* $Cd_{55}Mg_{35}Tb_{10}$ QC (Sato et al., 2002) found no long-range magnetic order down to 2.5 K and significant short-range spin correlations at low temperatures. These short-range spin correlations turned out to be very

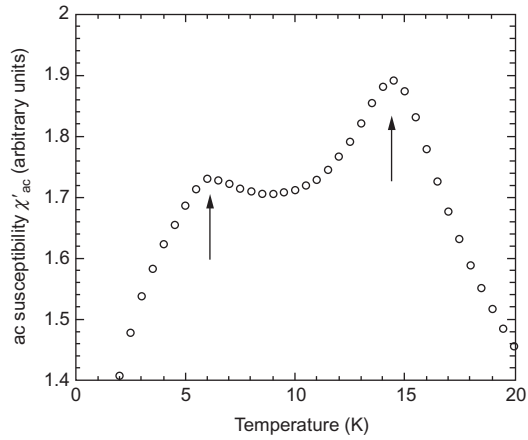

Figure 2.32 The temperature dependence of the ac susceptibility of the polygrain *i* $Cd_{55}Mg_{35}Tb_{10}$ QC measured at a frequency of 10 Hz in a zero-bias field and a 1-Oe ac magnetic field (Sato et al., 2001).

similar to the correlations found for the polygrain *i* $Zn_{60}Mg_{30}Tb_{10}$ QC (Sato et al., 1998b, 2000b).

Dolinšek et al. (2003) carried out TRM decay experiments for the polygrain *i* $Cd_{50}Mg_{40}Tb_{10}$ QC with two freezing temperatures (Figs. 2.30 and 2.32), studied earlier by Sato et al. (2001). The same time and field dependences of the TRM were observed (Dolinšek et al., 2003), as those for the single-grain *i* $Zn_{56.8}Mg_{34.6}Tb_{8.7}$ QC (Dolinšek et al., 2001). It was concluded (Dolinšek et al., 2003) that the *i* Cd–Mg–Tb QCs should be viewed as superparamagnetic noninteracting clusters rather than as spin glasses.

4.3. Zn–Mg–Sc(Ga,Cu)

Discovered by Kaneko et al. (2001), the thermodynamically stable *i* Zn–Mg–Sc QC has a P-type 6D Bravais lattice and is of a high structural quality comparable to that of the best F-type *i* QCs (de Boissieu et al., 2005). Figure 2.33 shows the temperature dependence of the magnetic susceptibility of the polygrain *i* $Zn_{80.5}Mg_{4.2}Sc_{15.3}$ QC (Motomura et al., 2004). The decrease in the susceptibility with increasing temperature below 100 K is of the Curie–Weiss type and is probably due to magnetic impurities (inset in Fig. 2.33). The susceptibility increase with increasing temperature above 150 K was accounted for by the temperature dependence of Pauli paramagnetism (Motomura et al., 2004). The $\chi(T)$ data were fitted to the relation

$$\chi = \chi_0 + \frac{C}{T-\theta} + AT^2, \tag{3}$$

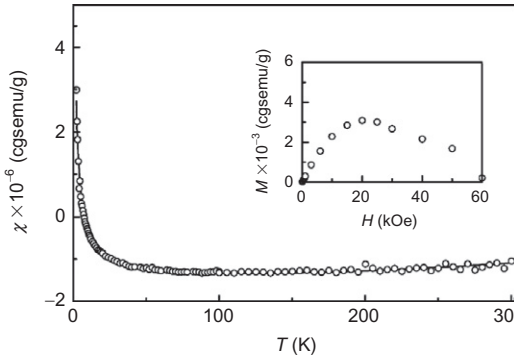

Figure 2.33 The temperature dependence of the magnetic susceptibility of the polygrain *i* $Zn_{80.5}Mg_{4.2}Sc_{15.3}$ QC. The solid line is the fit to Eq. (3). The inset shows the field dependence of the magnetization at 2 K (Motomura et al., 2004).

in which the term proportional to T^2 accounts for the temperature dependence of Pauli paramagnetism and

$$A = \frac{\mu_B^2 N(E_F)(\pi k_B)^2}{3}\left[\frac{1}{N(E_F)}\left(\frac{d^2N(E_F)}{dE_F^2}\right) - \left(\frac{1}{N(E_F)}\frac{dN(E_F)}{dE_F}\right)^2\right], \qquad (4)$$

where $N(E_F)$ is the electronic density of states (DOS) and E_F is the Fermi energy at 0 K. The parameters obtained from the fit of the $\chi(T)$ data (Fig. 2.33) to Eq. (3) are listed in Table 2.4. The positive value of A indicates via Eq. (4) that $d^2N(E_F)/dE_F^2$ is positive, which implies the existence of a pseudogap in the DOS at E_F (Kobayashi et al., 1997).

Similar $\chi(T)$ data were obtained for the polygrain *i* $Zn_{40}Mg_{40}Ga_{20}$ QC that also has the P-type Bravais lattice (Saito et al., 1993). In particular, a T^2 dependence of $\chi(T)$ was observed and was interpreted as indirect evidence for the existence of a valley-like structure in the DOS near E_F.

The magnetic properties of the *i* Cu–Ga–Sc–Mg QCs of the P-type Bravais lattice were studied by Yamada et al. (2004). The $\chi(T)$ data for the polygrain *i* $Cu_{47.7}Ga_{33.3}Sc_{15}Mg_4$ and $Cu_{47.1}Ga_{32.9}Sc_{15}Mg_5$ QCs (Fig. 2.34) were fitted to Eq. (3) and the parameters obtained from the fit are listed in Table 2.5. A positive value of A obtained from the fits was interpreted as an indication of the presence of a pseudogap in the DOS at E_F.

4.4. Zn–Sc(Tm)–TM

New *i* QCs in the Zn–Sc–TM system were discovered by Maezawa et al. (2004). These QCs have the P-type Bravais lattice. Figure 2.35 shows the temperature dependence of the magnetic susceptibility for these QCs and

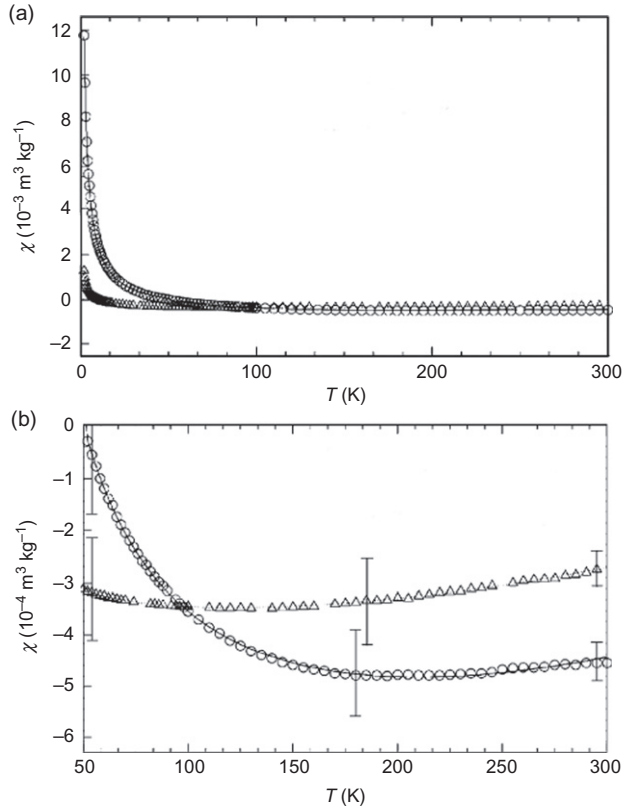

Figure 2.34 The temperature dependence of the magnetic susceptibility of the polygrain *i* QCs $Cu_{47.7}Ga_{33.3}Sc_{15}Mg_4$ (circles) and $Cu_{47.1}Ga_{32.9}Sc_{15}Mg_5$ (triangles) in the temperature range 2−300 K (a) and 50−300 K (b). The solid lines are the fits to Eq. (3) (Yamada et al., 2004).

Table 2.5 Parameters obtained from the fits of the $\chi(T)$ data to Eq. (3) for *i* QCs $Zn_{80.5}Mg_{4.2}Sc_{15.3}$, $Cu_{47.7}Ga_{33.3}Sc_{15}Mg_4$, and $Cu_{47.1}Ga_{32.9}Sc_{15}Mg_5$

Alloy	X_0 (10^{-7} emu/g)	C (10^{-6} emu K/g)	θ (K)	A (10^{-13} emu/g K^2)	References
$Zn_{80.5}Mg_{4.2}Sc_{15.3}$	−1.51	1.35	1.18	4.13	Motomura et al. (2004)
$Cu_{47.7}Ga_{33.3}Sc_{15}Mg_4$	−7.48	37	0.162	20	Yamada et al. (2004)
$Cu_{47.1}Ga_{32.9}Sc_{15}Mg_5$	−4.12	5.63	−10.82	13.3	Yamada et al. (2004)

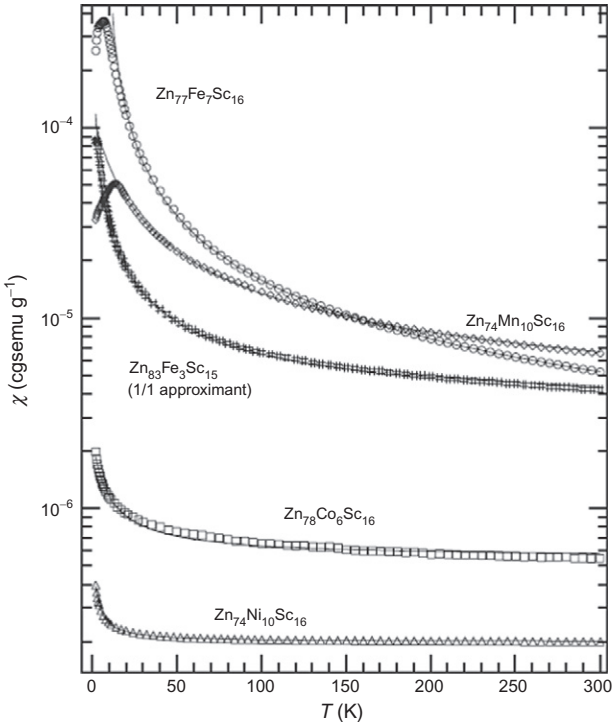

Figure 2.35 The temperature dependence of the magnetic susceptibility of the polygrain *i* QCs $Zn_{77}Sc_{16}Fe_7$, $Zn_{74}Sc_{16}Mn_{10}$, $Zn_{78}Sc_{16}Co_6$, $Zn_{74}Sc_{16}Ni_{10}$ and the polygrain 1/1 AP $Zn_{82}Sc_{15}Fe_3$, measured in an external magnetic field of 600 Oe (Kashimito et al., 2006).

the 1/1 AP $Zn_{82}Sc_{15}Fe_3$. The parameters obtained from the fits of the $\chi(T)$ data to Eq. (1) are listed in Table 2.6. It is noted that the Fe atoms in the *i* $Zn_{77}Sc_{16}Fe_7$ QC (Table 2.6) carry the largest magnetic moment $\mu_{\rm eff}^{\rm Fe}$ ever reported for an Fe-containing *i* QC, lying in the range 3.2–3.7 μ_B (the moment of 5.3 μ_B reported by Kashimito et al. (2004) is probably an outlier). The smaller $\mu_{\rm eff}^{\rm Fe}=2.3\mu_B$ found for the 1/1 AP (Table 2.6) is in good agreement with the value of $\sim 2\,\mu_B$ predicted by theoretical calculations carried out for the cubic Zn–Sc–Fe AP (Ishii et al., 2006). As illustrated in Fig. 2.36, two *i* QCs, $Zn_{77}Sc_{16}Fe_7$ and $Zn_{74}Sc_{16}Mn_{10}$, and the 1/1 AP $Zn_{82}Sc_{15}Fe_3$, exhibit spin-glass ordering.

The temperature dependence of the ac susceptibility of the polygrain *i* $Zn_{77}Sc_{16}Fe_7$ QC measured at different frequencies is shown in Fig. 2.37. A sharp peak in $\chi'(T)$, the position of which defines T_f, shifts to higher temperatures with increasing frequencies (Fig. 2.37a), a behavior typical of conventional spin glasses (Mydosh, 1993). The out-of-phase susceptibility χ' vanishes above T_f, but is nonzero for temperatures just below T_f (Fig. 2.37b),

Table 2.6 Parameters obtained from the fits of the $\chi(T)$ data to the modified Curie–Weiss law for the polygrain *i* Zn–Sc–TM QCs and the 1/1 AP $Zn_{82}Sc_{15}Fe_3$

Alloy	X_0 (10^{-6} emu/g)	θ (K)	$\mu_{eff}^{TM}(\mu_B)$	T_f (K)	References
$Zn_{77}Sc_{16}Fe_7$	0.209	6.54	5.3	7.2	Kashimito et al. (2004)
	−0.357	4.2	3.7	7.0	Kashimito et al. (2006)
	0.19(3)	3(1)	3.23(2)	7	Sato et al. (2008)
	10.7(1)	10.6(2)	3.55(1)	7.75(2)	Al-Qadi et al. (2009)
$Zn_{74}Sc_{16}Mn_{10}$	2.86	−9.3	0.31	14.0	Kashimito et al. (2006)
$Zn_{78}Sc_{16}Co_6$	0.552	−4.7	0.27		Kashimito et al. (2006)
$Zn_{74}Sc_{16}Ni_{10}$	0.199	−0.8	0.07		Kashimito et al. (2006)
$Zn_{82}Sc_{15}Fe_3$	0.333	−0.9	2.3	2.5	Kashimito et al. (2006)

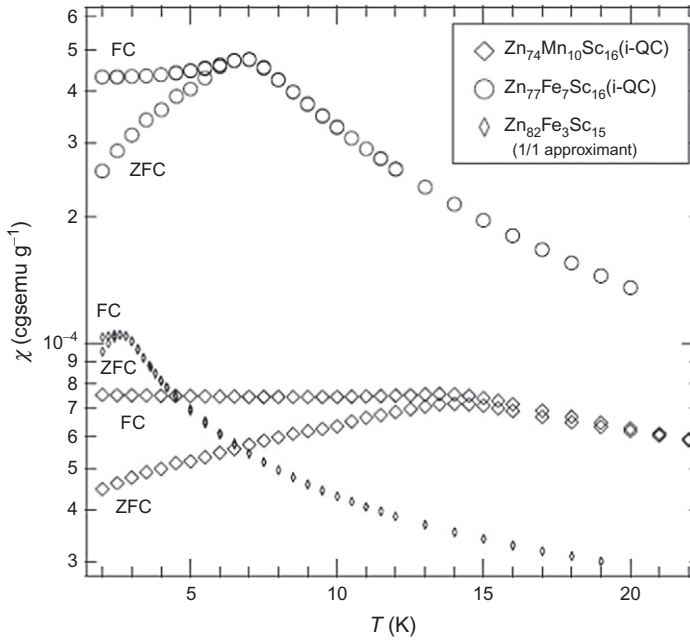

Figure 2.36 The temperature dependence of the ZFC and FC magnetic susceptibility of the *i* QCs $Zn_{77}Sc_{16}Fe_7$, $Zn_{74}Sc_{16}Mn_{10}$ and the AP $Zn_{82}Sc_{15}Fe_3$, measured in an external magnetic field of 50 Oe (Kashimito et al., 2006).

which implies dissipation not only at the freezing transition but also at temperatures below it, a common feature of spin glasses (Mydosh, 1993). The observed change of T_f with f corresponds to $K = 0.016(1)$, which is a factor of 3 smaller than the K value for the *i* $Zn_{56.8}Mg_{34.6}Tb_{8.7}$ QC (Fisher et al., 1999).

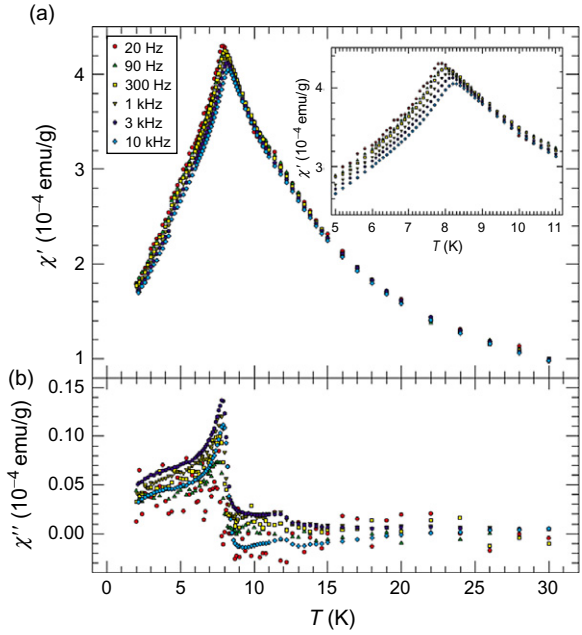

Figure 2.37 The temperature dependence of the (a) in-phase magnetic susceptibility χ' and (b) out-of-phase magnetic susceptibility χ'' for different frequencies from 20 to 10 kHz for the *i* $Zn_{77}Sc_{16}Fe_7$ QC. The inset in (a) is a magnification around the maximum in χ' (Al-Qadi et al., 2009).

The $T_f(f)$ data for the *i* $Zn_{77}Sc_{16}Fe_7$ QC were fitted (Fig. 2.38) to Eq. (2) yielding $f_0 = 7.20(22) \times 10^{11}$ Hz, $E_a/k_B = 25.1(2.6)$ K, and $T_0 = 6.87(47)$ K. The values of f_0, E_a/k_B, and T_0 are similar to those found for other spin-glass systems (Mydosh, 1993).

The use of Eq. (2) to fit the $T_f(f)$ implies a cluster model interpretation of the spin-freezing phenomenon in a spin glass in which the system is considered as a set of interacting superparamagnetic clusters (Al-Qadi et al., 2009). The other interpretation of the spin-freezing phenomenon assumes the occurrence of a true phase transition (Al-Qadi et al., 2009). The frequency-dependent maximum of $\chi'(T)$ indicates the freezing temperature T_f where the maximum relaxation time, τ, of the system is equal to the characteristic time $1/f$ set by the frequency of the ac-susceptibility measurement. The scaling theory near the phase transition at T_c predicts that the temperature dependence of τ obeys the power-law divergence:

$$\tau = \tau_0 \left(\frac{T_f - T_c}{T_c} \right)^{zv}, \quad T_f > T_c, \tag{5}$$

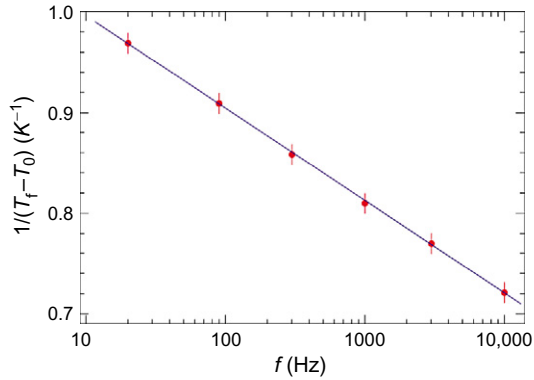

Figure 2.38 The frequency dependence of the freezing temperature T_f for the *i* $Zn_{77}Sc_{16}Fe_7$ QC. The solid line is the best fit to Eq. (2) (Al-Qadi et al., 1999).

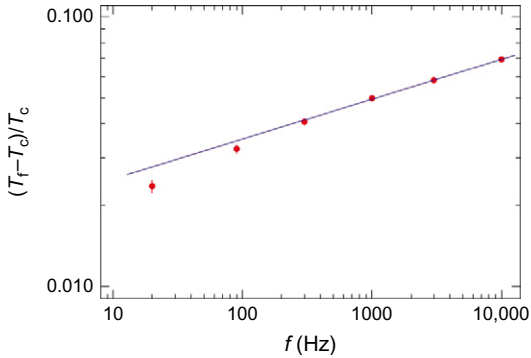

Figure 2.39 The frequency dependence of the freezing temperature T_f for the *i* $Zn_{77}Sc_{16}Fe_7$ QC. The solid line is the best fit to Eq. (5) (Al-Qadi et al., 1999).

where τ_0 is the microscopic relaxation time, z is the dynamic exponent relating the correlation length ξ and τ as $\tau \propto \xi^z$, and ν is the critical exponent for the correlation length $\propto /((T_f/T_c) - 1)^{-\nu}$. The best fit of the $T_f(f)$ data (Fig. 2.39) to Eq. (5) gives $\tau_0 = 1.47(32) \times 10^{-12}$ s, $T_c = 7.72(8)$ K, and $z\nu = 6.77(1.14)$ (Al-Qadi et al., 1999). The derived values of τ_0 and $z\nu$ are similar to those reported for canonical $Cu_{1-x}Mn_x$ spin glasses. One notes that the fit of the $T_f(f)$ data to Eq. (5) (Fig. 2.39) is worse than the fit to Eq. (2) (Fig. 2.38). It would thus appear that the spin freezing in the *i* $Zn_{77}Sc_{16}Fe_7$ QC is a nonequilibrium phenomenon rather than a phase transition.

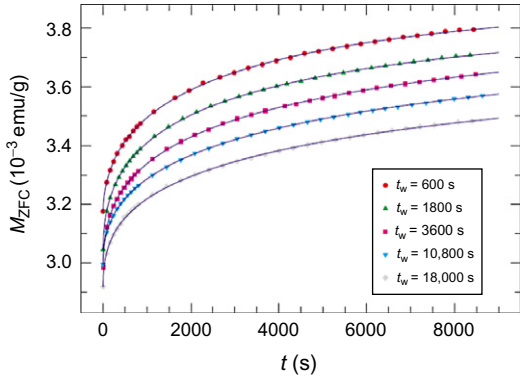

Figure 2.40 The time dependence of the ZFC magnetization for an applied magnetic field of 20 Oe at 4.8 K for different waiting times t_w of the *i* $Zn_{77}Sc_{16}Fe_7$ QC (Al-Qadi et al., 2009).

The spin-glass nature of the *i* $Zn_{77}Sc_{16}Fe_7$ QC was probed by studying aging effects via ZFC magnetization decay and TRM decay measurements (Al-Qadi et al., 2009). A ZFC magnetization decay experiment involves cooling the sample in zero magnetic field from above T_f to the measurement temperature T_m below T_f, allowing the sample to stay at T_m for a certain waiting time t_w, and then applying a small magnetic field and recording the change in magnetization with time. Figure 2.40 shows the ZFC decays at $T_m = 4.8\ \text{K} = 0.62\ T_f$ and in the magnetic field of 20 Oe for different waiting times. It is evident from the figure that the ZFC magnetization strongly depends on t_w: the longer the t_w is, the slower is the decay of the ZFC magnetization. The system becomes "stiffer" for longer waiting times. The observed dependence of the ZFC magnetization is the same as that observed for canonical spin glasses (Mydosh, 1993).

The TRM decays for different waiting times at a cooling field of 50 K, and at $T_m = 4.8\ \text{K} = 0.62\ T_f$ and $T_m = 6.0\ \text{K} = 0.77\ T_f$ are shown in Fig. 2.41. One finds that (i) the TRM decreases strongly as T_f is approached, (ii) the larger the t_w, the larger the TRM, and (iii) the time decay of the TRM slows down as t_w increases. These three dependences are exactly the same as those observed for canonical spin glasses and are compatible with the dynamics of a spin-glass system in an ultrametrically organized free-energy landscape (Al-Qadi et al., 2009; Dolinšek et al., 2003).

The existence of the ultrametrically organized phase space in a spin glass can also be probed by studying the TRM decay as a function of the cooling field. Figure 2.42 shows the decay of the TRM for $t_w = 3600$ s at $T_m = 4.8\ \text{K} = 0.62\ T_f$ and $T_m = 6.0\ \text{K} = 0.77\ T_f$ as a function of the cooling

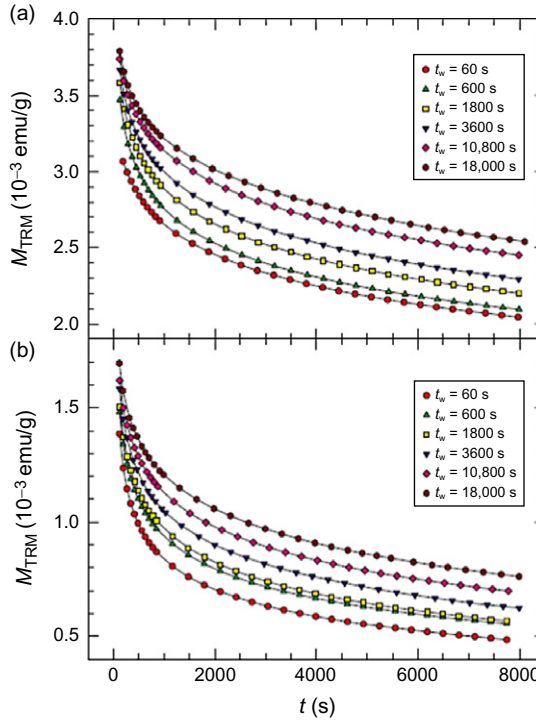

Figure 2.41 The TRM time decays at an applied magnetic field of 50 Oe for different waiting times t_w at (a) 4.8 and (b) 6.0 K of the *i* $Zn_{77}Sc_{16}Fe_7$ QC (Al-Qadi et al., 2009).

field *H*. One can observe that the magnitude of the TRM increases with the cooling field. But such a TRM dependence on *H* is exactly opposite to that observed for a canonical spin glass where the TRM decreases with *H* (Al-Qadi et al., 2009). It was then concluded (Al-Qadi et al., 2009) that the nature of the spin-glass state in the *i* $Zn_{77}Sc_{16}Fe_7$ QC is fundamentally different from that of a canonical spin glass.

Kashimito et al. (2007) discovered that *i* QCs with the P-type Bravais lattice can be formed in the $Zn_{77}Sc_{16-x}RE_xFe_7$ (RE = Ho, Er, Tm) system. The magnetic properties of the *i* $Zn_{77}Sc_{16-x}Tm_xFe_7$ QCs were studied by Kashimito et al. (2007, 2009). These QCs seem to be spin glasses (Figs. 2.43 and 2.44) with the T_f values listed in Table 2.7. A comparison between the measured Curie constants *C* and the calculated C_{cal} (under the assumption that only the Tm atoms carry a magnetic moment of 7.56 μ_B) shows that $C > C_{cal}$ (Table 2.6). This indicates that Fe atoms must also carry a magnetic moment in these QCs.

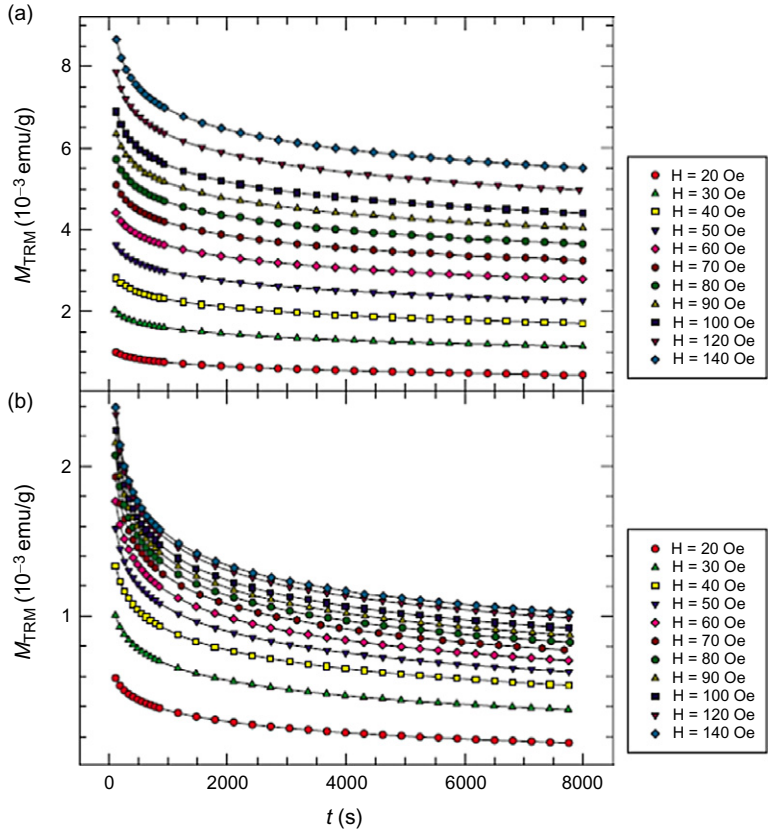

Figure 2.42 The TRM time decays for $t_w = 3600$ s at (a) 4.8 and (b) 6.0 K for different cooling fields H of the *i* $Zn_{77}Sc_{16}Fe_7$ QC (Al-Qadi et al., 2009).

4.5. Binary systems

The magnetic properties of the binary polygrain *i* $Cd_{5.7}Yb$ QC and its 1/1 AP Cd_6Yb were studied by Dhar et al. (2002). The temperature dependence of the magnetic susceptibility of these two alloys is shown in Fig. 2.45. The magnetic susceptibility of these two alloys is diamagnetic at 300 K with a value of -8.32×10^{-5} and -2.14×10^{-5}, respectively. The sharp increase in χ of the *i* $Cd_{5.7}Yb$ QC and the 1/1 AP Cd_6Yb below 80 and 240 K was attributed to the presence of magnetic impurities (Dhar et al., 2002).

The magnetic susceptibility of the 1/1 AP Cd_6Yb (Yamada et al., 2010), which is a 1/1 AP to the recently discovered *i* $Zn_{88}Sc_{12}$ QC (Canfield et al., 2010), is negative in the temperature range 1.8–300 K, which indicates that this AP is a diamagnet.

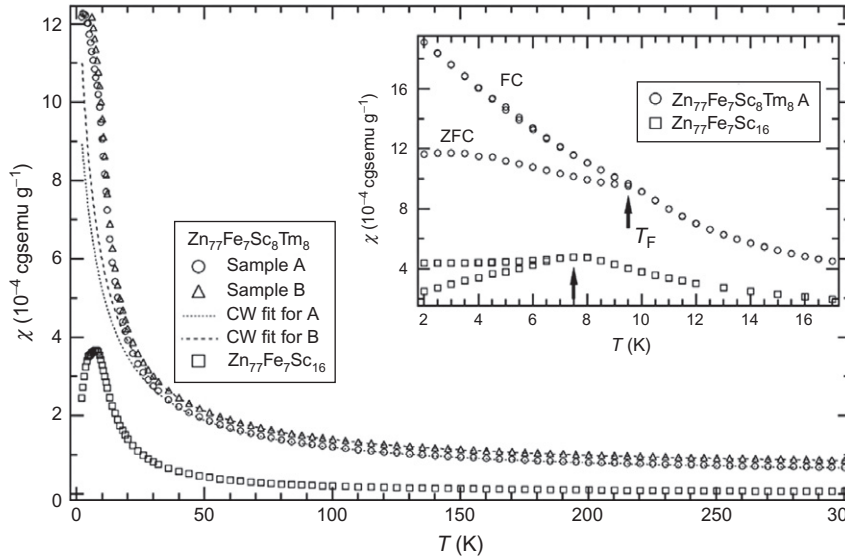

Figure 2.43 The temperature dependence of the magnetic susceptibility of the polygrain *i* QCs $Zn_{77}Sc_{16}Fe_7$ and $Zn_{77}Sc_8Tm_8Fe_7$ measured in an external magnetic field of 300 Oe. The inset shows the temperature dependence of the ZFC and FC magnetic susceptibility measured in an external magnetic field of 50 Oe (Kashimito et al., 2007).

Binary alloys Cd_6M (M = Sr, Y, Ce, Pr, Nd, Sm, Eu, Gd, Tb, Dy, Ho, Er, Tm, Lu, Np) are the 1/1 APs (Gómez and Lidin, 2003) to the yet to be discovered binary Cd–M QCs. Some of these APs exhibit a long-range antiferromagnetic order. For instance, Cd_6Eu (Buschow and van Steenwijk, 1977) and Cd_6Tb (Tamura et al., 2010) are antiferromagnets with the T_N of 2.25(5) and 24 K, respectively. This suggests that a long-range quasiperiodic antiferromagnetic order may be possible in the corresponding binary *i* Cd–M QCs.

4.6. Ag–In–RE

The discovery of the first thermodynamically stable binary *i* QCs $Cd_{5.7}Yb$ and $Cd_{5.7}Ca$ by Tsai et al. (2000) and Guo et al. (2000b) has led to the finding of many ternary *i* QCs by total or partial replacement of Yb or Ca and Cd with other elements. In particular, by replacing Yb with RE elements and Cd with Ag and In, a series of new *i* Ag–In–RE was discovered (Guo and Tsai, 2000; Iwano et al., 2006). A similar replacement in the Cd_6Yb AP of Yb with RE elements and Cd with Ag and In has led to the discovery of ternary Ag–In–RE 1/1 APs to the *i* Ag–In–RE QCs (Iwano et al., 2006; Ruan et al., 2004). Magnetic properties of several polygrain

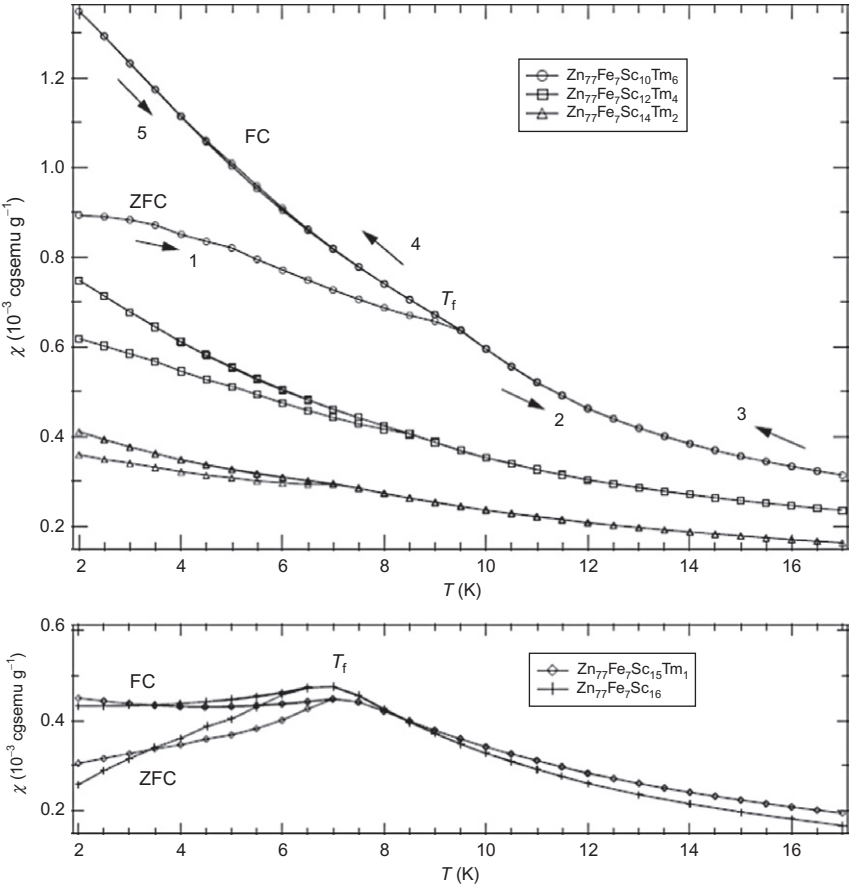

Figure 2.44 The temperature dependence of the ZFC and FC magnetic susceptibility of the polygrain *i* QCs $Zn_{77}Sc_{16-x}Tm_xFe_7$ with $x = 0$, 1, 2, 4, and 6 measured in an external magnetic field of 50 Oe (Kashimito et al., 2009).

Ag–In–RE APs were studied by Wang et al. (2009), Ibuka et al. (2011), and Wang et al. (2011). Magnetism of one *i* QC $Ag_{50}In_{36}Gd_{14}$ was investigated by Stadnik et al. (2007) and Wang et al. (2009).

Figures 2.46 and 2.47 show the temperature dependence of the magnetic susceptibility of the $Ag_{50}In_{36}Gd_{14}$ *i* QC and its 1/1 AP, respectively. The $\chi(T)$ data could be well fitted (Fig. 2.46a and b) to Eq. (1) with the parameters listed in Table 2.8. For both alloys, the negative values of θ indicate an antiferromagnetic coupling between the Gd magnetic moments, and the closeness of the μ_{eff}^{Gd} values to the theoretical value of 7.94 μ_B for a free Gd^{3+} ion shows that the Gd magnetic moments are well localized. The $\chi(T)$ data for other Ag–In–RE APs (Ibuka et al. 2011; Wang et al., 2011)

Table 2.7 Parameters obtained from the fits of the $\chi(T)$ data to the modified Curie–Weiss law for the polygrain *i* QCs $Zn_{77}Sc_{16-x}Tm_xFe_7$ with $x = 0, 1, 2, 4$, and 6

Alloy	X_0 (10^{-7} emu/g)	C (10^{-3} emu K/g)	C_{cal} (10^{-3} emu K/g)	θ (K)	T_f (K)	References
$Zn_{77}Sc_{15}Tm_1Fe_7$	5.04	2.53	1.14	2.6	7.0(5)	Kashimito et al. (2009)
$Zn_{77}Sc_{14}Tm_2Fe_7$	1.55	3.39	2.24	−4.9	7.0(5)	Kashimito et al. (2009)
$Zn_{77}Sc_{12}Tm_4Fe_7$	6.84	5.47	4.32	−7.5	8.0(5)	Kashimito et al. (2009)
$Zn_{77}Sc_{10}Tm_6Fe_7$	1.04	7.50	6.24	−9.9	8.5(5)	Kashimito et al. (2009)
$Zn_{77}Sc_8Tm_8Fe_7$	3.9 5.8	8.7 8.7	8.03	−8.2 −6.3	9.0(5) 9.0(5)	Kashimito et al. (2009) Kashimito et al. (2007)

C_{cal} is the Curie constant calculated under the assumption that only Tm atoms carry a magnetic moment of 7.56 μ_B.

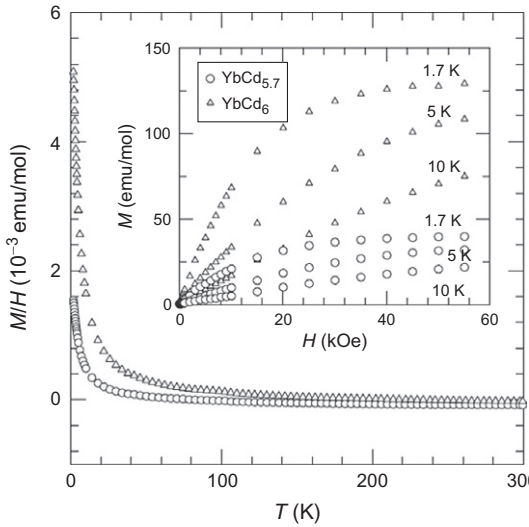

Figure 2.45 The temperature dependence of the magnetic susceptibility of the polygrain *i* $Cd_{5.7}Yb$ QC and its 1/1 AP Cd_6Yb measured in an external magnetic field of 20 kOe. The inset shows the magnetization versus applied magnetic field at several temperatures (Dhar et al., 2002).

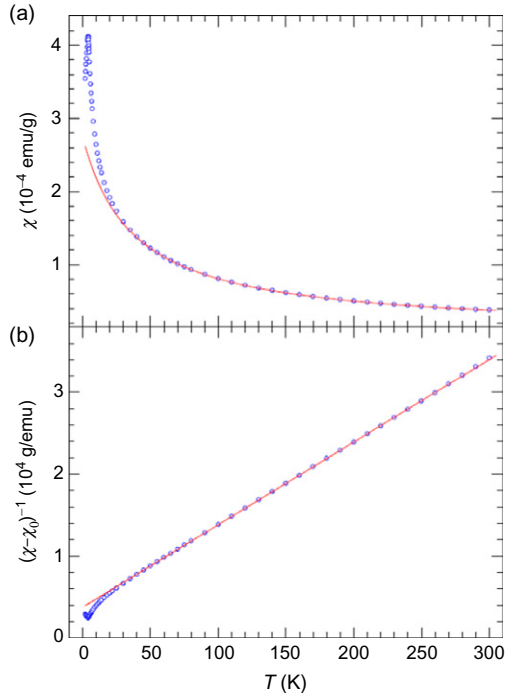

Figure 2.46 (a) The temperature dependence of the magnetic susceptibility of the *i* $Ag_{50}In_{36}Gd_{14}$ QC measured in an external magnetic field of 30 Oe. The solid line is the fit to Eq. (1) in the temperature range 50–300 K. (b) The inverse magnetic susceptibility corrected for the contribution χ_0, $(\chi-\chi_0)^{-1}$ versus T of the *i* $Ag_{50}In_{36}Gd_{14}$ QC. The solid line is the fit to Eq. (1) (Stadnik et al., 2007).

could also be well fitted to Eq. (1) and the corresponding parameters are given in Table 2.8. One notices that θ is negative for all studied Ag–In–RE APs, except for the Ag–In–Eu AP, which confirms the expected antiferromagnetic interaction between the RE magnetic moments. Also, the values of $\mu_{\mathrm{eff}}^{\mathrm{RE}}$ are quite close the theoretical values for free RE^{3+} ions (and RE^{2+} for RE = Eu), which confirms the localized and isotropic nature of the RE magnetic moments.

The ZFC and FC $\chi(T)$ data for the *i* $Ag_{50}In_{36}Gd_{14}$ QC (Fig. 2.48), its 1/1 AP (Fig. 2.49) and the $Ag_{46.4}In_{39.7}Tb_{13.9}$ AP (Fig. 2.50) indicate that these alloys are spin glasses with the corresponding freezing temperatures given in Table 2.8. The spin-glass ordering in the *i* $Ag_{50}In_{36}Gd_{14}$ QC and its 1/1 AP was confirmed by ac magnetic susceptibility measurements (Figs. 2.51 and 2.52). Spin freezing in the $Ag_{50}In_{36}Gd_{14}$ AP (Fig. 2.52)

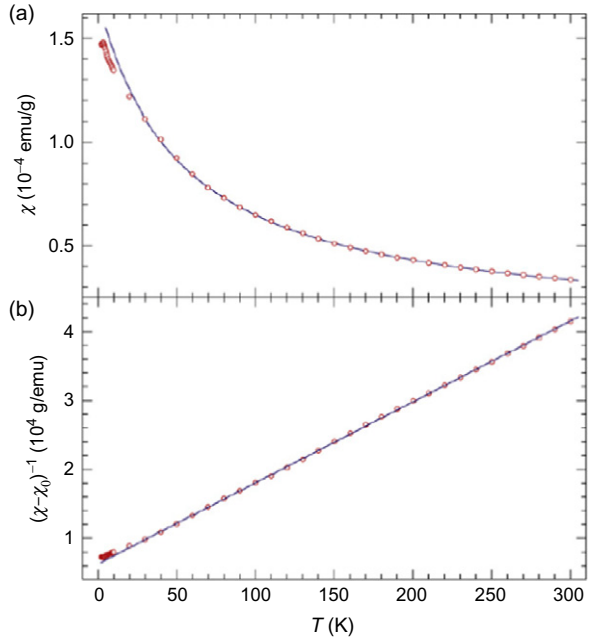

Figure 2.47 (a) The temperature dependence of the magnetic susceptibility of the $Ag_{50}In_{36}Gd_{14}$ AP measured in an external magnetic field of 50 Oe. The solid line is the fit to Eq. (1) in the temperature range 70–300 K. (b) The inverse magnetic susceptibility corrected for the contribution χ_0, $(\chi-\chi_0)^{-1}$ versus T of the $Ag_{50}In_{36}Gd_{14}$ AP. The solid line is the fit to Eq. (1) (Wang et al., 2009).

Table 2.8 Parameters obtained from the fits of the $\chi(T)$ data to the modified Curie–Weiss law for the polygrain Ag–In–RE APs and the *i* $Ag_{50}In_{36}Gd_{14}$ and $Ag_{42}In_{42}Yb_{16}$ QCs

Alloy	θ (K)	$\mu_{\text{eff}}^{\text{RE}}(\mu_B)$	$\mu_{\text{th}}^{\text{RE}}(\mu_B)$	T_f (K)	References
$Ag_{46.9}In_{38.7}Nd_{14.4}$	−23.23(18)	4.543	3.62		Ibuka et al. (2011)
$Ag_{43.1}In_{43.8}Eu_{13.1}$	6(16)	8.2(8)	7.94[a]	2.5	Ibuka et al. (2011)
$Ag_{46.7}In_{39.2}Gd_{14.1}$	−55.5(9)	8.89(3)	7.94	3.3(1)	Ibuka et al. (2011)
$Ag_{50}In_{36}Gd_{14}$	−55.9(2)	7.64(9)		3.7(1), 2.4(1)	Wang et al. (2009)

Continued

Table 2.8 (*Continued*)

Alloy	θ (K)	$\mu_{\text{eff}}^{\text{RE}}(\mu_B)$	$\mu_{\text{th}}^{\text{RE}}(\mu_B)$	T_f (K)	References
i $Ag_{50}In_{36}Gd_{14}$	−37.1(2)	8.15(1)		4.25(5)	Stadnik et al. (2007)
$Ag_{42}In_{42}Gd_{16}$	−73.6(5)	7.86(23)		3.6(1)	Wang et al. (2011)
$Ag_{46.4}In_{39.7}Tb_{13.9}$	−34.13(14)	10.77(7)	9.72	3.7	Ibuka et al. (2011)
$Ag_{47.2}In_{38.2}Dy_{14.5}$	−17.69(18)	11.262(10)	10.65	2.5	Ibuka et al. (2011)
$Ag_{43}In_{41}Ho_{16}$	−12.09(12)	11.638(7)	10.61		Ibuka et al. (2011)
$Ag_{45}In_{40}Er_{15}$	−5.58(18)	9.746	9.58		Ibuka et al. (2011)
$Ag_{42.2}In_{42.6}Tm_{15.2}$	−3.96(6)	8.490(4)	7.56		Ibuka et al. (2011)
i $Ag_{42}In_{42}Yb_{16}$	−0.8[b] −0.8[c] −0.8[d]	0.27[b] 0.41[c] 0.22[d]	4.54		Bobnar et al. (2011)

[a]For Eu^{2+}.
[b]Along the twofold direction.
[c]Along the threefold direction.
[d]Along the fivefold direction.

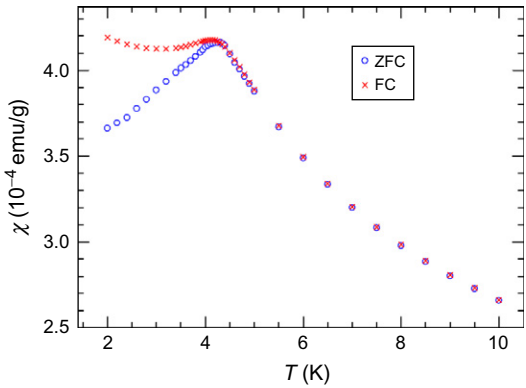

Figure 2.48 The temperature dependence of the ZFC and FC magnetic susceptibility of the *i* $Ag_{50}In_{36}Gd_{14}$ QC measured in an external magnetic field of 30 Oe (Stadnik et al., 2007).

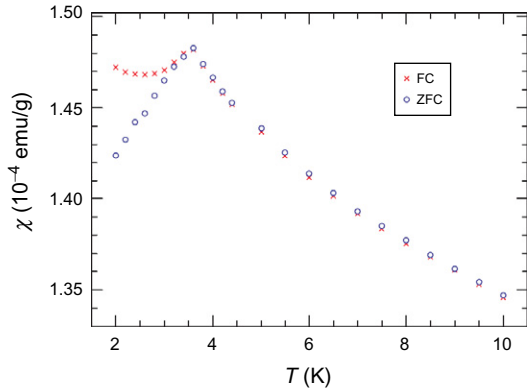

Figure 2.49 The temperature dependence of the ZFC and FC magnetic susceptibility of the $Ag_{50}In_{36}Gd_{14}$ AP measured in an external magnetic field of 50 Oe (Wang et al., 2009).

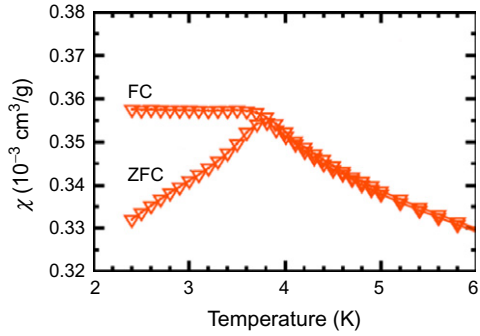

Figure 2.50 The temperature dependence of the ZFC and FC magnetic susceptibility of the $Ag_{46.4}In_{39.7}Tb_{13.9}$ AP measured in an external magnetic field of 100 Oe (Ibuka et al., 2011).

appears to be a two-stage process, although one cannot exclude the possibility that the anomaly in the $\chi'(T)$ data at 2.6 K is due to the presence of a magnetic impurity. The observed change in T_f with f in the *i* $Ag_{50}In_{36}Gd_{14}$ QC and its 1/1 AP can be accounted for better with the Vogel–Fulcher law than with the dynamics of critical slowing down (Wang et al., 2009). This indicates that in both alloys spin freezing is not a true equilibrium phase transition but rather a nonequilibrium phenomenon.

The frustration parameter f for the *i* $Ag_{50}In_{36}Gd_{14}$ QC and the Ag–In–RE APs is very large (Table 2.8). Thus, similar to the *i* Zn–Mg–RE and Cd–Mg–RE QCs, they can be regarded as geometrically frustrated magnets.

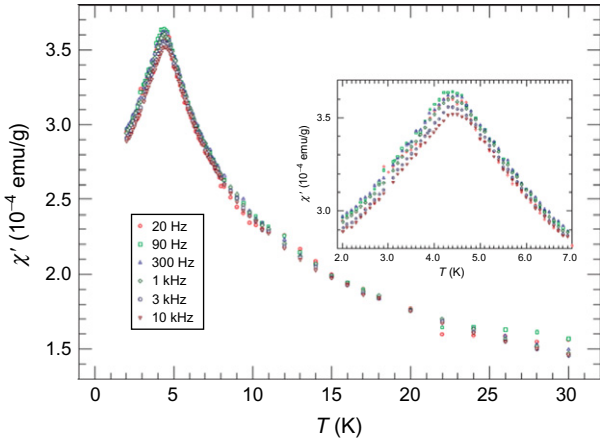

Figure 2.51 The temperature dependence of the in-phase magnetic susceptibility χ' for different applied frequencies from 20 to 10 kHz for the *i* $Ag_{50}In_{36}Gd_{14}$ QC. The inset is a magnification around the maximum in χ' (Wang et al., 2009).

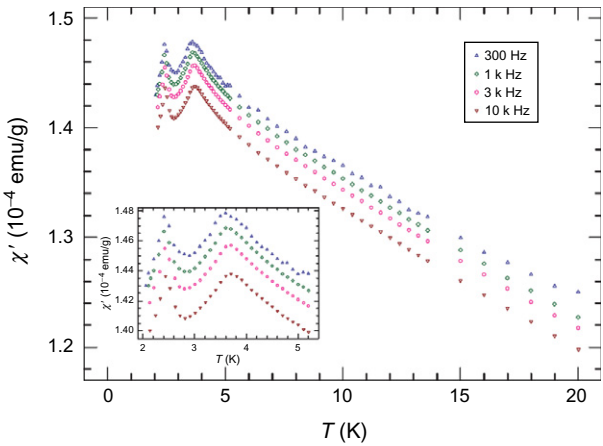

Figure 2.52 The temperature dependence of the in-phase magnetic susceptibility χ' for different applied frequencies from 300 to 10 kHz for the $Ag_{50}In_{36}Gd_{14}$ AP. The inset shows a magnification of the low-temperature region (Wang et al., 2009).

Neutron scattering experiments were done on the $Ag_{46.4}In_{39.7}Tb_{13.9}$ AP by Ibuka et al. (2011). The absence of magnetic Bragg reflections (Fig. 2.53a) confirmed that there is no long-range magnetic order in the $Ag_{46.4}In_{39.7}Tb_{13.9}$ AP. The presence of the diffuse scattering peaks (Fig. 2.53b) indicates the existence of short-range spin correlations with

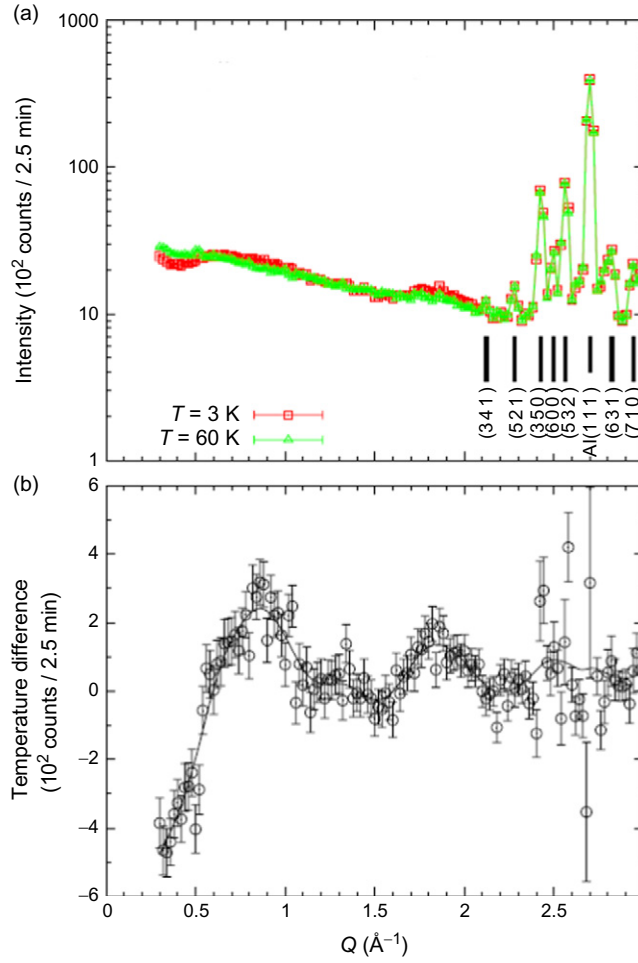

Figure 2.53 The neutron diffraction patterns at 3 and 60 K (a) and the difference between the neutron diffraction patterns at 3 and 60 K (b) for the $Ag_{46.4}In_{39.7}Tb_{13.9}$ AP. The vertical lines in (a) refer to the nuclear Bragg positions. The solid line in (b) is a guide to the eye (Ibuka et al., 2011).

an estimated correlation length of about 9 Å, which is close to the 11-Å diameter of a single *i* cluster of Tb atoms in this AP (Ibuka et al., 2011). A broad peak at about 4 meV was observed in the neutron inelastic scattering spectra of the $Ag_{46.4}In_{39.7}Tb_{13.9}$ AP (Ibuka et al., 2011). Its presence allowed Ibuka et al. (2011) to argue that spin freezing occurs in two stages. At temperatures much above T_f, spatial correlations between the spins in an *i* cluster start to develop and with further cooling, fluctuations of the *i* spin

clusters themselves slow down and eventually freeze at T_f. This interpretation of the freezing phenomenon in the $Ag_{46.4}In_{39.7}Tb_{13.9}$ AP is essentially the same as that used for the *i* Zn–Mg–Ho(Tb) QCs (Sato, 2005; Sato et al., 2000b, 2006) and the *i* $Cd_{55}Mg_{35}Tb_{10}$ QC (Sato et al., 2002).

Magnetic properties of the single-grain *i* $Ag_{42}In_{42}Yb_{16}$ QC were studied by Bobnar et al. (2011). The *i* $Ag_{42}In_{42}Yb_{16}$ QC is a weak paramagnet. The fits of the $\chi(T)$ data to Eq. (1) yield the parameters listed in Table 2.8. The very small value of $\mu_{\mathrm{eff}}^{\mathrm{Yd}}$ as compared to the theoretical value of 4.54 μ_B for a free Yb^{3+} ion was interpreted as resulting from a small fraction (on the order of 10^{-3}) of the magnetic Yb^{3+} moments diluted in the sea of the nonmagnetic Yb^{2+} ions.

5. Summary

All known QCs are either paramagnets, diamagnets, or spin glasses. Ferromagnetic order reported for several QCs is most probably of extrinsic origin. Only neutron diffraction experiments on such QCs could determine the existence of long-range ferromagnetic order. Similarly, the antiferromagnetic order reported for the polygrain *i* Zn–Mg–RE QCs was convincingly demonstrated to result from magnetic impurities.

The main difficulty in demonstrating the existence of the theoretically expected long-range magnetic order in QCs comes from the fact that the studied polygrain samples almost unavoidably contain magnetically ordered impurity phase(s). It seems that the experiments aimed at detecting long-range magnetic order in QCs should be conducted on single-grain samples. Such samples can be grown for many potentially magnetically ordered QCs.

In several QCs, the spin-glass dynamics probed via aging experiments seems to be very different from that expected in a canonical spin glass. This difference deserves further experimental and theoretical investigations.

ACKNOWLEDGMENT

This work was supported by the Natural Sciences and Engineering Research Council of Canada.

REFERENCES

Al-Qadi, K., Wang, P., Stadnik, Z.M., Przewoźnik, J., 2009. Phys. Rev. B **79**, 224202, and references therein.

Bahadur, D., Srivastava, C.M., Yewondwossen, M.H., Dunlap, R.A., 1995. J. Phys. Condens. Matter **7**, 9883.

Beckman, O., Lundgren, L., 1991. In: Buschow, K.H.J. (Ed.), Handbook of Magnetic Materials Vol. 6, North-Holland, Amsterdam, p. 181.
Bhattacharjee, S.M., Ho, J.-S., Johnson, A.A.Y., 1987. J. Phys. A **20**, 4439.
Bihar, Ž., Bilušić, A., Lukatela, J., Smontara, A., Jeglič, P., McGuiness, P.J., Dolinšek, J., Jagličić, Z., Janovec, J., Demange, V., Dubois, J.M., 2006. J. Alloys Compd. **407**, 65.
Binder, K., Young, A.P., 1986. Rev. Mod. Phys. **58**, 801.
Bobnar, M., Vrtnik, S., Jagličić, Z., Wenecka, M., Cui, C., Tsai, A.P., Dolinšek, J., 2011. Phys. Rev. B **84**, 134205.
Buschow, K.H.J., van Steenwijk, F.J., 1977. Phys. B **85**, 122.
Cahn, J.W., Shechtman, D., Gratias, D., 1986. J. Mater. Res **1**, 13.
Canfield, P.C., Caudle, M.I., Ho, C.-S., Kreyssig, A., Nandi, S., Kim, M.G., Lin, X., Kracher, A., Dennis, K.W., McCallum, R.W., Goldman, A.I., 2010. Phys. Rev. B **81**, 020201(R).
Charrier, B., Schmitt, D., 1997. J. Magn. Magn. Mater **171**, 106.
Charrier, B., Ouladdiaf, B., Schmitt, D., 1997. Phys. Rev. Lett. **78**, 4637.
Cyrot-Lackmann, F., 1997. Solid State Commun. **103**, 123.
de Boissieu, M., Francoual, S., Kaneko, Y., Ishimasa, T., 2005. Phys. Rev. Lett. **95**, 105503.
Dhar, S.K., Palenzona, A., Manfrinetti, P., Pattalwar, S.M., 2002. J. Phys. Condens. Matter **14**, 517.
Dolinšek, J., Jagličić, Z., Chernikov, M.A., Fisher, I.R., Canfield, P.C., 2001. Phys. Rev. B **64**, 224209.
Dolinšek, J., Jagličić, Z., Sato, T.J., Guo, J.Q., Tsai, A.P., 2003. J. Phys. Condens. Matter **15**, 7981.
Dolinšek, J., Vrtnik, S., Smontara, A., Jagodič, M., Jagličić, Z., Bauer, B., Gille, P., 2008a. Philos. Mag. **88**, 2145.
Dolinšek, J., Slanovec, J., Jagličić, Z., Heggen, M., Balanetskyy, S., Feuerbacher, M., Urban, K., 2008b. Phys. Rev. B **77**, 064430.
Duneau, M., Dunlop, F., Jagannathan, A., Oguey, C., 1991. Mod. Phys. Lett. B **5**, 1895.
Elser, V., 1985. Phys. Rev. B **32**, 4892.
Escudero, R., Lasjaunias, J.C., Calvayrac, Y., Boudard, M., 1999. J. Phys. Condens. Matter **11**, 383.
Fisher, I.R., Isalm, Z., Panchula, A.F., Cheon, K.O., Kramer, M.J., Canfield, P.C., Goldman, A.I., 1998. Philos. Mag. B **77**, 1601.
Fisher, I.R., Cheon, K.O., Panchula, A.F., Canfield, P.C., Chernikov, M., Ott, H.R., Dennis, K., 1999. Phys. Rev. B **59**, 308.
Godrèche, C., Luck, J.M., Orland, H., 1986. J. Stat. Phys. **45**, 777.
Goldman, A.I., Kelton, K.F., 1993. Rev. Mod. Phys. **65**, 213.
Gómez, C.P., Lidin, S., 2003. Phys. Rev. B **68**, 2003.
Guo, J.Q., Tsai, A.P., 2000. Philos. Mag. Lett. **82**, 349.
Guo, J., Abe, E., Tsai, A.-P., 2000a. Jpn. J. Apply. Phys **39**, L770.
Guo, J., Abe, E., Tsai, A.P., 2000b. Phys. Rev. B **62**, R14605.
Hafner, J., Krajčí, M., 1998. Phys. Rev. B **58**, 2849.
Hattori, Y., Niikura, A., Tsai, A.P., Inoue, A., Masumoto, T., Fukamichi, K., Aruga-Katori, H., Goto, T., 1995. J. Phys. Condens. Matter **7**, 2313.
Hermisson, J., 2000. J. Phys. A **33**, 57.
Hida, K., 2001. Phys. Rev. Lett. **86**, 1331.
Hippert, F., Préjean, J.J., 2008. Philos. Mag. **88**, 2175, and references therein.
Hippert, F., Simonet, V., de Laissardière, Trambly, Audier, M., Calvayrac, Y., 1999. J. Phys. Condens. Matter **11**, 10419.
Hippert, F., Audier, M., Préjean, J.J., Sulpice, A., Lhotel, E., Simonet, V., Calvayrac, Y., 2003. Phys. Rev. B **68**, 134402.
Hundley, M.F., McHenry, M.E., Dunlap, R.A., Srinivas, V., 1992. Philos. Mag. B **66**, 239.

Ibuka, S., Iida, K., Sato, T.J., 2011. J. Phys. Condens. Matter **23**, 056001.
Ishii, Y., Nozawa, K., Fujiwara, T., 2006. Philos. Mag. **86**, 693.
Islam, Z., Fisher, I.R., Zarestky, J., Canfield, P.C., Stassis, C., Goldman, A.I., 1998. Phys. Rev. B **57**, R11047.
Iwano, S., Nishimoto, K., Tamura, R., Takeuchi, S., 2006. Philos. Mag. **86**, 435.
Jagannathan, A., 2004. Phys. Rev. Lett. **92**, 047202.
Jagannathan, A., 2005. Phys. Rev. **71**, 115101.
Jagannathan, A., Schulz, H.J., 1997. Phys. Rev. B **55**, 8045.
Jagannathan, A., Szallas, A., 2009. Z. Kristallogr. **224**, 53.
Jagannathan, A., Szallas, A., Wessel, S., Duneau, M., 2007. Phys. Rev. B **75**, 212407.
Janot, C., 1994. Quasicrystals: A Primer. Oxford University Press, Oxford.
Kaneko, Y., Arichika, Y., Ishimasa, T., 2001. Philos. Mag. Lett. **81**, 7777.
Kashimito, S., Matsuo, S., Nakano, H., Shimizu, T., Ishimasa, T., 1999. Solid State Commun. **109**, 63.
Kashimito, S., Motomura, S., Maezawa, R., Matsuo, S., Ishimasa, T., 2004. Jpn. J. Appl. Phys. **43**, L526.
Kashimito, S., Motomura, S., Francoual, S., Matsuo, S., Ishimasa, T., 2006. Philos. Mag. **86**, 725.
Kashimito, S., Masuda, C., Motomura, S., Matsuo, S., Ishimasa, T., 2007. Philos. Mag. **87**, 2929.
Kashimito, S., Masuda, C., Ishimasa, T., 2009. Z. Kristallogr. **224**, 59.
Kimura, K., Kishi, K., Hashimoto, T., Takeuchi, S., Shibuya, T., 1991. Mater. Sci. Eng. A **133**, 94.
Klein, T., Gozlan, A., Berger, C., Cyrot-Lackmann, F., Calvayrac, Y., Quivy, A., Fillion, G., 1990. Phys. B **165–166**, 283.
Klein, T., Berger, C., Mayou, D., Cyrot-Lackmannm, F., 1991. Phys. Rev. Lett. **66**, 2907.
Kobayashi, A., Matsuo, S., Ishimasa, T., Nakano, H., 1997. J. Phys. Condens. Matter **9**, 3205.
Krajčí, M., Hafner, J., 1998. Phys. Rev. B **58**, 14110.
Lasjaunias, J.C., Sulpice, A., Keller, N., Préjean, J.J., de Boissieu, M., 1995. Phys. Rev. B **52**, 886.
Ledue, D., Teillet, J., Carnet, J., Dujardin, J., 1993. J. Non-Cryst. Solids **153–154**, 403.
Lévy, L.P., 1988. Phys. Rev. B **38**, 4963, and references therein.
Lifshitz, R., 1998. Phys. Rev. Lett. **80**, 2717.
Lifshitz, R., 2000. Mater. Sci. Eng. A **294–296**, 508.
Lifshitz, R., Mandel, S.E.-D., 2004. Acta Crystallogr. A **60**, 167.
Lin, C.R., Lin, C.M., Lin, S.T., Lyubutin, I.S., 1995a. Phys. Lett. A **196**, 365.
Lin, C.R., Lin, S.T., Lyubutin, I.S., 1995b. J. Magn. Magn. Mater. **151**, 155.
Lundgren, L., Svendlinh, P., Nordblad, P., Beckman, O., 1983. Phys. Rev. Lett. **51**, 911.
Lyubutin, I.S., Lin, Ch.R., Lin, S.T., 1997. J. Exp. Theor. Phys. **84**, 800.
Lück, R., Kek, S., 1993. J. Non-Cryst. Solids **153–154**, 329.
Maezawa, R., Kashimoto, S., Ishimasa, T., 2004. Philos. Mag. Lett. **84**, 2004.
Mandel, S.E.-D., Lifshitz, R., 2004. Acta Crystallogr. A **60**, 179.
Martin, S., Hebard, A.F., Kortan, A.R., Thiel, F.A., 1991. Phys. Rev. Lett. **67**, 719.
Matsuo, S., Ishimasa, T., Nakano, H., Fukano, Y., 1988. J. Phys. F **18**, L175.
Matsuo, S., Ishimasa, T., Mori, M., Nakano, H., 1992. J. Phys. Condens. Matter **4**, 10053.
Matsuo, S., Ishimasa, T., Nakano, H., 2000. Mater. Sci. Eng. A **294–296**, 633.
Matsuo, S., Ishimasa, T., Nakano, H., 2002. J. Magn. Magn. Mater. **246**, 223.
Matsuo, S., Nakano, H., Motomura, S., Ishimasa, T., 2005. J. Phys. Soc. Jpn. **74**, 1036.
Matsuo, S., Motomura, S., Ishimasa, T., 2007. Philos. Mag. **87**, 51.
Motomura, S., Kaneko, Y., Kashimoto, S., Nakano, H., Ishimasa, T., Matsuo, S., 2004. J. Non-Cryst. Solids **334–335**, 393.

Mydosh, J.A., 1993. Spin Glasses: An Experimental Introduction. Taylor and Francis, London.
Nasu, S., Miglierini, M., Kuwano, T., 1992. Phys. Rev. B **45**, 12778.
Niikura, A., Tsai, A.P., Inoue, A., Masumoto, T., 1994. Philos. Mag. Lett. Mag. Lett. **69**, 351.
O'Handley, R.C., Dunlap, R.A., McHenry, M.E., 1991. In: Buschow, K.H.J., Handbook of Magnetic Materials Vol. 6, North-Holland, Amsterdam p. 453.
Okabe, Y., Niizeki, K., 1988a. J. Phys. Soc. Jpn. **57**, 16.
Okabe, Y., Niizeki, K., 1988b. J. Phys. Soc. Jpn. **57**, 1536.
Peng, D.-L., Sumiyama, K., Suzuki, K., Inoue, A., Yokoyama, Y., Fukaura, K., Sunada, H., 1998. J. Magn. Magn. Mater. **184**, 319.
Préjean, J.J., Lhotel, E., Sulpice, A., Hippert, F., 2006. Phys. Rev. B **73**, 214205.
Ramirez, A.P., 2001. In: Buschow, K.H.J., (Ed.). Handbook of Magnetic Materials Vol. 13, North-Holland, Amsterdam p. 423.
Rau, D., Gavilano, J.L., Mushkolaj, Sh., Beeli, C., Chernikov, M.A., Ott, H.R., 2003. Phys. Rev. B **68**, 134204.
Reid, R.W., Bose, S.K., Mitrović, B., 1998. J. Phys. Condens. Matter **10**, 2303.
Reisser, R., Kronmüller, H., 1994. J. Magn. Magn. Mater. **131**, 90.
Ruan, J.F., Kuo, K.H., Guo, J.Q., Tsai, A.P., 2004. J. Alloys Compd. **370**, L23.
Saito, K., Matsuo, S., Ishimasa, T., 1993. J. Phys. Soc. Jpn. **62**, 604.
Sato, T.J., 2005. Acta Crystallogr. A **61**, 39.
Sato, T.J., Takakura, H., Tsai, A.P., 1998a. Jpn. J. Appl. Phys. **37**, L663.
Sato, T.J., Takakura, H., Tsai, A.P., Shibata, K., 1998b. Phys. Rev. Lett. **81**, 2364.
Sato, T.J., Takakura, H., Tsai, A.P., Ohoyama, K., Shibata, K., Andersen, K.H., 2000a. Mater. Sci. Eng. A **294–296**, 481.
Sato, T.J., Takakura, H., Tsai, A.P., Shibata, K., Ohoyama, K., Andersen, K.H., 2000b. Phys. Rev. B **61**, 476.
Sato, T.J., Guo, J., Tsai, A.P., 2001. J. Phys. Condens. Matter **13**, L105.
Sato, T.J., Takakura, H., Guo, J., Tsai, A.P., Ohoyama, K., 2002. J. Alloys Compd. **342**, 365.
Sato, T.J., Takakura, H., Tsai, A.P., Shibata, K., 2006. Phys. Rev. B **73**, 054417.
Sato, T.J., Kashimoto, S., Masuda, C., Onimaru, T., Nakanowatari, I., Iida, K., Morinaga, R., Ishimasa, T., 2008. Phys. Rev. B **77**, 014437.
Sebastian, S.E., Huie, T., Fisher, I.R., Dennis, K.W., Kramer, M.J., 2004. Philos. Mag. **84**, 1029.
Shechtman, D., Blech, I., Gratias, D., Cahn, J.W., 1984. Phys. Rev. Lett. **53**, 1951.
Smontara, A., Smiljanić, I., Ivkov, J., Stanić, D., Barišić, O.S., JagličićGille, P., Komelj, M., Jeglič, P., Bobnar, M., Dolinšek, J., 2008. Phys. Rev. B **78**, 104204.
Stadnik, Z.M., (Ed.) (1999). *In* "Physical Properties of Quasicrystals". Springer-Verlag, Berlin.
Stadnik, Z.M., Müller, F., 1995. Philos. Mag. B **71**, 221.
Stadnik, Z.M., Stroink, G., 1991. Phys. Rev. B **43**, 894, and references therein.
Stadnik, Z.M., Stroink, G., Ma, H., Williams, G., 1989. Phys. Rev. B **39**, 9797.
Stadnik, Z.M., Müller, F., Goldberg, F., Rosenberg, M., Stroink, G., 1993. J. Non-Cryst. Solids **156–158**, 909.
Stadnik, Z.M., Purdie, D., Baer, Y., Lograsso, T.A., 2001. Phys. Rev. B **64**, 214202.
Stadnik, Z.M., Al-Qadi, K., Wang, P., 2007. J. Phys. Condens. Matter **19**, 326208.
Steurer, W., 2004. Z. Kristallogr. **219**, 391.
Steurer, W., Deloudi, S., 2008. Acta Crystallogr. A **64**, 1.
Steurer, W., Deloudi, S., 2009. Crystallography of Quasicrystals. Springer-Verlag, Berlin.
Swenson, C.A., Lograsso, T.A., Anderson, N.E. Jr., Ross, A.R., 2004. Phys. Rev. B **70**, 094201.

Szallas, A., Jagannathan, A., 2008. Phys. Rev. B **77**, 104427.
Szallas, A., Jagannathan, A., Wessel, S., 2009. Phys. Rev. B **79**, 172406.
Tamura, R., Muro, Y., Hiroto, T., Nishimoto, K., Takabatake, T., 2010. Phys. Rev. B **82**, 220201(R).
Tobo, A., Onodera, H., Yamaguchi, Y., Yokoyama, Y., Note, R., Inoue, A., 2001. Hyperfine Interact. **133**, 27.
Toulouse, G., 1977. Commun. Phys. **2**, 116.
Tsai, A.P., Inoue, A., Masumoto, T., 1987. Jpn. J. Appl. Phys. **26**, L1505.
Tsai, A.-P., Inoue, A., Masumoto, T., Kataoka, N., 1988. Jpn. J. Appl. Phys. **27**, L2252.
Tsai, A.P., Niikura, A., Inoue, A., Masumoto, T., Nishida, Y., Tsuda, K., Tanaka, M., 1994. Philos. Mag. Lett. Mag. Lett. **70**, 169.
Tsai, A.P., Guo, J.Q., Abe, E., Takakura, H., Sato, T.J., 2000. Nature **408**, 537.
Vedmedenko, E.Y., 2004. Ferroelectrics **305**, 129.
Vedmedenko, E.Y., 2005. Mod. Phys. Lett. B **19**, 1367.
Vedmedenko, E.Y., Oepen, H.P., Kirschner, J., 2003. Phys. Rev. Lett. **90**, 137203.
Vedmedenko, E.Y., Grimm, U., Wiesendanger, R., 2004. Phys. Rev. Lett. **93**, 076407.
Vedmedenko, E.Y., Grimm, U., Wiesendanger, R., 2006. Philos. Mag. **86**, 733.
Velikov, Yu.Kh., Salikhov, S.V., Isaev, E.I., Johansson, B., 2005a. J. Exp. Theor. Phys. **100**, 1127.
Velikov, Yu.Kh., Isaev, E.I., Johansson, B., 2005b. Solid State Commun. **133**, 473.
Wang, P., Stadnik, Z.M., Al-Qadi, K., Przewoźnik, J., 2009. J. Phys. Condens. Matter **21**, 436007.
Wang, P., Stadnik, Z.M., Przewoźnik, J., 2011. J. Alloys Compd. **509**, 3435.
Wen, Z., Ma, J., Fu, X., 2008. Solid State Commun. **146**, 304.
Wessel, S., Milat, I., 2005. Phys. Rev. B **71**, 104427.
Wessel, S., Jagannathan, A., Haas, S., 2003. Phys. Rev. Lett. **90**, 177205.
Yamada, Y., Yokoyama, Y., Matono, K.-I., Fukaura, K., Sunada, H., 1999. Jpn. J. Appl. Phys. **38**, 52.
Yamada, H., Motomura, S., Maezawa, R., Kaneko, Y., Ishimasa, T., Nakano, H., Matsuo, S., 2004. J. Non-Cryst. Solids **334–335**, 398.
Yamada, T., Tamura, R., Muro, Y., Motoya, K., Isobe, M., Ueda, Y., 2010. Phys. Rev. B **82**, 134121.
Yamamoto, A., Takakura, H., 2008. Quasicrystals. In: Fujiwara, T. and Ishii, Y., (Eds.), Quasicrystals. Elsevier, Amsterdam p. 11.
Yokoyama, Y., Inoue, A., 1996a. Mater. Trans. JIM **37**, 339.
Yokoyama, Y., Inoue, A., 1996b. Jpn. J. Appl. Phys. **35**, 559.
Yokoyama, Y., Inoue, A., Yamauchi, H., Kusuyama, M., Masumoto, T., 1994. Jpn. J. Appl. Phys. **33**, 4012.
Yokoyama, Y., Yamada, Y., Fukaura, K., Sunada, H., Inoue, A., Note, R., 1997. Jpn. J. Appl. Phys. **36**, 6470.